MT Bilimsel™

www.mtbilimsel.com

Yer Altı Kaynakları Dergisi | *Journal of Underground Resources*

Yıl:6 | Sayı:11 | Ocak 2017

Year:6 | Number:11 | January 2017

ISSN: 2146-9431

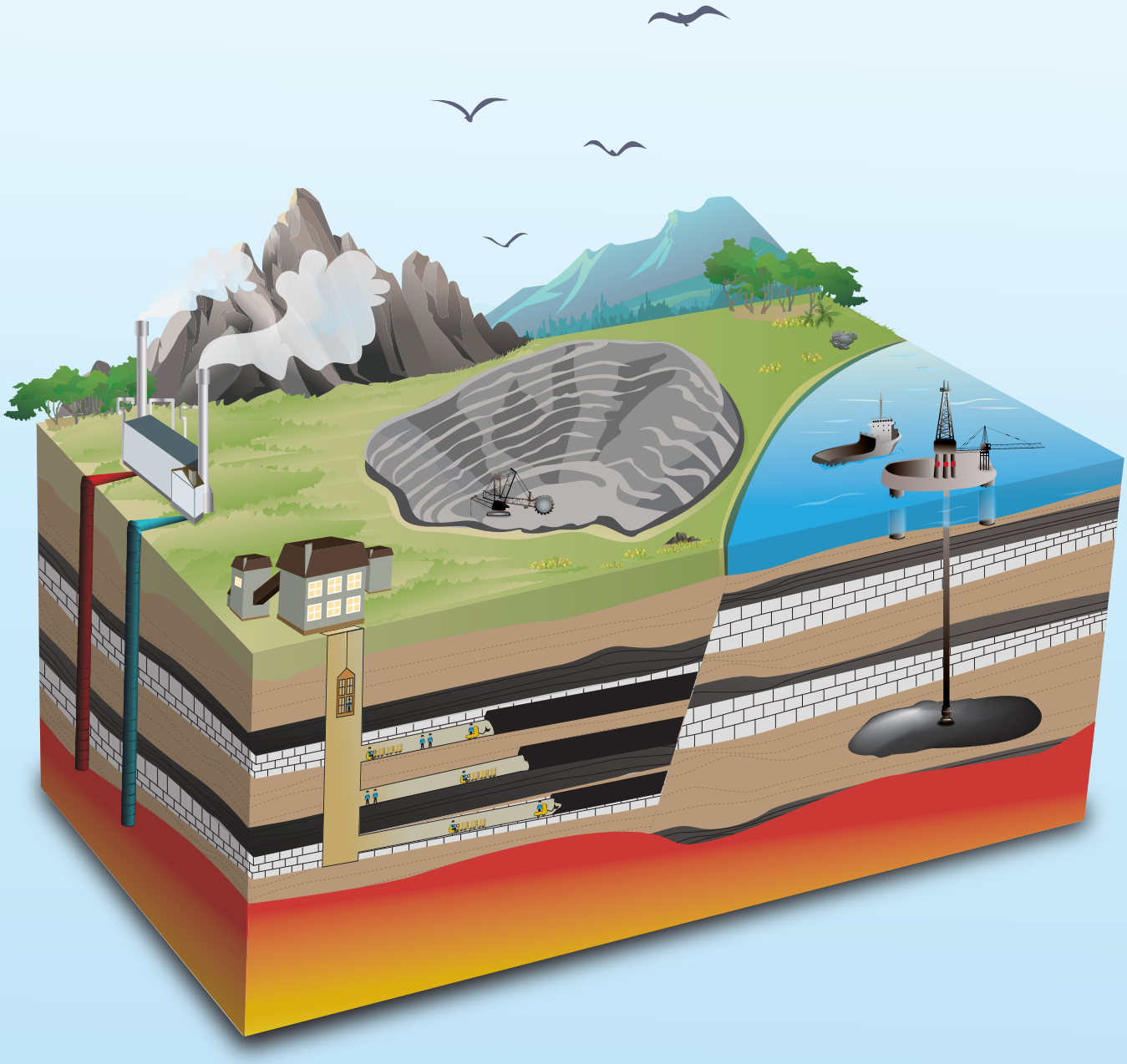

MT Bilimsel

Yer Altı Kaynakları Dergisi | *Journal of Underground Resources*

Derginin Adı
MT Bilimsel

İmtiyaz Sahibi
MAYEB Madencilik ve Yer Bilimleri Basım Yayın Dağıtım Ltd. Şti.
adına Onur Aydın

Genel Koordinatör
Onur Aydın
onur@mtbilimsel.com

Yazı İşleri Müdürü
O. Çağım Tuğ
cagim@madencilik-turkiye.com

Yurtdışı İlişkiler
Eray İmgel
eray@madencilik-turkiye.com

İdari İşler
Volkan Okyay
volkan@madencilik-turkiye.com

Grafik Tasarım - Uygulama
Gökçe Çınar
gokce@madencilik-turkiye.com

İnternet Teknolojileri
Bilgin B. Yılmaz
bilgin@madencilik-turkiye.com

Hukuk Danışmanı
Av. Evrim İnal
evrim@madencilik-turkiye.com

Yayın İdare Merkezi
1042. Cd. (Eski 4. Cd.) 1335. Sk. (Eski 19. Sk.) Vadi Köşk Apt. No: 6/8 A. Öveçler ANK.
Tel : +90 (312) 482 18 60
Fax : +90 (312) 482 18 61

info@mtbilimsel.com
www.mtbilimsel.com

Yerel Süreli Yayındır

ISSN 2146-9431

Ulusal Hakemli Dergidir

Yayın Kurulu

MT Bilimsel™

www.mtbilimsel.com

Yer Altı Kaynakları Dergisi | *Journal of Underground Resources*

Yıl:6 | Sayı:11 | Ocak 2017 ISSN: 2146-9431

Year:6 | Number:11 | January 2017

İçindekiler

MT Bilimsel™
Yıl:6 | Sayı:11 | Ocak 2017
Year:6 | Number:11 | January 2017
Yer Altı Kaynakları Dergisi | *Journal of Underground Resources* **www.mtbilimsel.com**

Editor Ofisinden: MT Bilimsel Dergisi Uluslararası Karadeniz Madencilik ve Tünelcilik Sempozyumu Özel Sayısı

Editorial: MT Scientifc Journal Special Issue of International Black Sea Mining & Tunnelling Symposium

Kerim Aydıner [1], Serdar Yaşar [1], Özüm Yaşar [1], C. Okay Aksoy [2], Eren Kömürlü [3]
[1] MT Bilimsel Dergisi Uluslararası Karadeniz Madencilik ve Tünelcilik Sempozyumu Özel Sayısı Editörü, KTÜ Maden Mühendisliği Bölümü, Trabzon, Türkiye
[2] MT Bilimsel Dergisi Baş Editörü, DEÜ Maden Mühendisliği Bölümü, İzmir, Türkiye
[3] MT Bilimsel Dergisi Yardımcı Editörü, KTÜ Maden Mühendisliği Bölümü, Trabzon, Türkiye

Madencilik Türkiye Bilimsel (MT Bilimsel) dergisinin 11. sayısı, 2-4 Kasım 2016 tarihleri arasında Trabzon'da KTÜ Maden Mühendisliği Bölümü ve KTÜ Maden Derneği tarafından düzenlenen Uluslararası Karadeniz Madencilik ve Tünelcilik Sempozyumu bildirileri arasından seçilen çalışmaları içermektedir. Bu sayıda sempozyumun ana temaları olan tünelcilik, madencilik, cevher hazırlama ve zenginleştirme konularından seçilen altı adet tam metin bildiri yer almıştır. Bu özel sayının çıkarılmasında emeği geçen Madencilik Türkiye Bilimsel (MT Bilimsel) dergisinin tüm kadrosuna teşekkürlerimizi sunarız. Ayrıca sempozyumun başarıya ulaşmasındaki emeklerinden dolayı sempozyum organizasyon komitesi üyelerine, bilim kurulu üyelerine, yazarlara, katılımcılara ve emeği geçen herkese teşekkürlerimizi sunarız.

This 11th Issue of Mining Turkey Scientific (MT Bilimsel) Journal includes selected papers from proceedings of International Black Sea Mining and Tunnelling Symposium which was organized by Karadeniz Technical University Mining Engineering Department and Karadeniz Technical University Mining Association in Trabzon, on 2-4 November 2016. In this issue, six proceedings were published from the topics of tunnelling, mining and mineral processing which are the main themes of the Symposium. We hereby thank to all crew of Mining Turkey Scientific (MT Bilimsel) Journal of Underground Resources for their generous helps during publication of this special issue. Additionally, we would like to acknowledge all the organizing committee, scientific committee, authors, participants, and all people who contributed for the success of the Symposium.

Makale Gönderim Tarihi: 13.07.2016
Yayına Kabul Tarihi: 20.08.2016

Engineering Geological Assessment and Preliminary Support Design for Cankurtaran Tunnel, NE Turkey

Ayberk Kaya [1]*, Fikri Bulut [2]
[1] *Recep Tayyip Erdogan University, Department of Geological Engineering, Rize*
[2] *Karadeniz Technical University, Department of Geological Engineering, Trabzon*
**Corresponding Author: ayberk.kaya@erdogan.edu.tr*

Abstract
The main purpose of this study is to determine the geotechnical properties of the rock masses and to suggest the convenient support design for the Cankurtaran (Hopa-Artvin) tunnel, NE Turkey. The detailed geotechnical investigations were carried to define the rock masses that mainly consist of sedimentary, pyroclastic, and volcanic units. Empirical and numerical methods were utilized and results were compared for safe tunnel design. The RMR, Q, and NATM systems were used as empirical methods to characterize the rock masses and to determine the support design. The performance of suggested support design, induced stress distributions and deformations were controlled using the finite element method (FEM). It was concluded that the empirical support design was not successful to prevent deformations developed around the tunnel in very poor rock masses under great in-situ rock stresses. Therefore, a new support design was suggested and, its performance was also checked using the FEM analyses. Finally, it is concluded that the empirical and numerical methods should be combined for more realistic and safe support design.

Keywords: Tunneling, Rock mass classification, Support design, FEM.

1. Introduction

In this study, the Cankurtaran tunnel (Figure 1) was selected as an application site for empirical and numerical tunnel support procedure. The detailed engineering geological investigations include field and laboratory studies followed by classification of rock masses and numerical modeling to determine the preliminary support design have been carried out. The field studies consisted of geological mapping, drillings, water pressure tests, scan-line surveys, and seismic investigations. The necessary support designs were estimated by means of the RMR, Q, and NATM systems. In addition to the empirical methods, the FEM based numerical analyses were also undertaken in order to define the stress distributions and deformations developed around the tunnel and to control the performance of empirical support design. Further, a new support design was recommended for unstable sections of the tunnel by the help of numerical analyses because designing a safer and economical support system is important in tunneling projects.

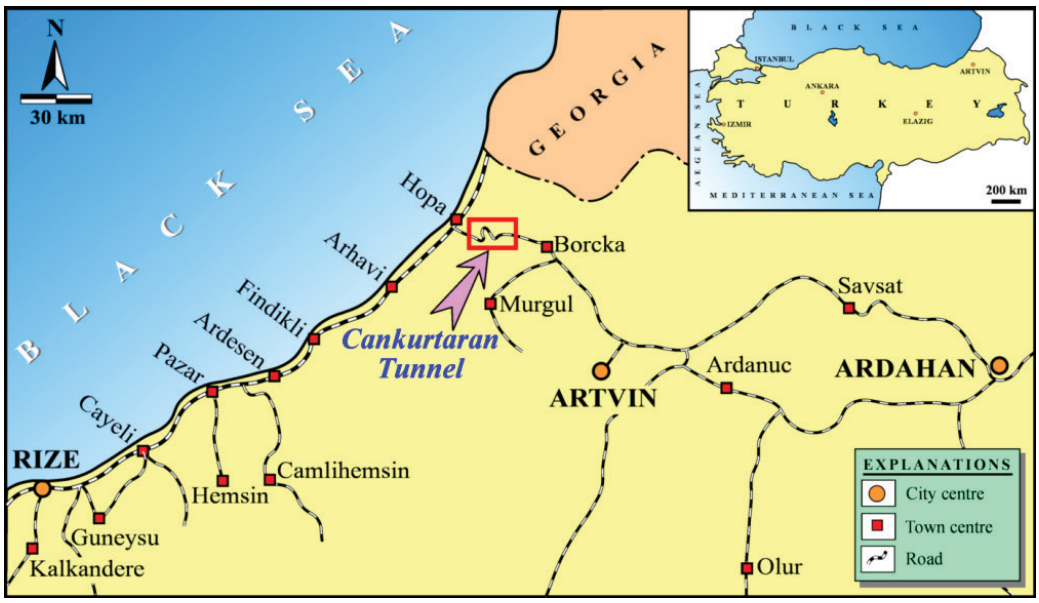

Figure 1. Location map of the study area

2. Geology of the Tunnel Alignment

In the study and surrounding area, geological units vary from old to young are the Late Cretaceous aged Subasi Ridge Formation, Late Cretaceous-Paleocene aged Cankurtaran Formation, Paleocene aged Senkaya Ridge Formation, Eocene aged Kabakoy Formation, and Quaternary aged alluvium (Capkinoglu, 1981; Guven, 1993; Kaya, 2012, Kaya and Bulut, 2013). The Subasi Ridge Formation is a volcano-sedimentary deposit characterized by the andesitic pyroclastites and intercalations of limestone, marl, sandstone, tuff, and siltstone. This formation is commonly exposed at the entrance section of the Cankurtaran tunnel comprising the study area. The Cankurtaran Formation consists of limestone and marly-limestone conformably overlies the Subasi Ridge Formation. This unit crops out in the inner section of the tunnel. Conformably overlying Senkaya Ridge Formation is composed of marl with various colors, limestone with partly red and gray laminate and intercalation of the claystone with thin and medium layered. This unit generally crops out towards the end of inner section of the tunnel. The Kabakoy Formation unconformably overlies the Senkaya Ridge Formation and lithologically consists of basalt, andesite, and their pyroclastites. The Quaternary aged alluvium is the youngest unit in the area. Each geological unit is shown in Figure 2 illustrates the geological cross-section.

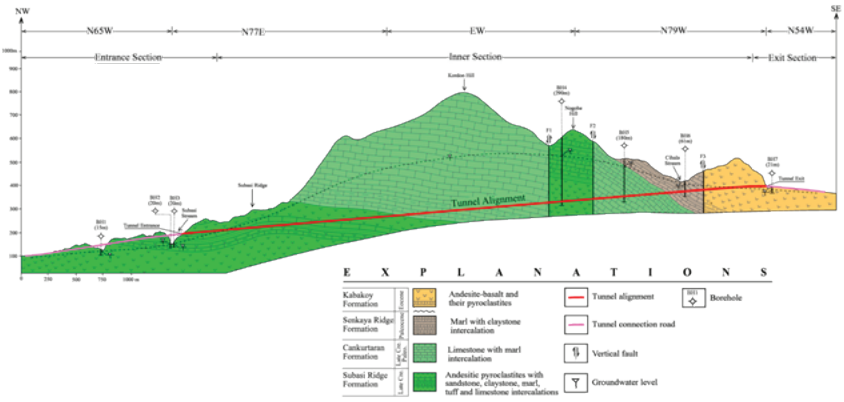

Figure 2. Geological cross-section showing the geological units along the tunnel alignment

3. Engineering Geological Investigations

Engineering geological properties of the rock masses crop out along the Cankurtaran tunnel alignment were determined in three stages comprising surface, subsurface, and laboratory studies. The field studies include detailed geological mapping, scan-line surveys, geophysical, and borehole investigations.

Seven investigation boreholes (Figure 2) having a total length of 607 m were drilled by Turkish General Directorate of Highways (KGM) in order to observe the rock mass characteristics at the tunnel level, to identify the discontinuity properties and groundwater level, sampling for the laboratory tests, and water pressure tests.

Laboratory tests were performed on the core samples taken from boreholes and rock blocks in accordance with the methods suggested by ISRM (2007) to determine the physico-mechanical and elastic properties of rock materials. Furthermore, the Rock Quality Designation (RQD) values were identified from boreholes and scan-line surveys using the techniques suggested by Deere (1964) and Priest and Hudson (1976).

The quantitative description of the discontinuities in the geotechnical units such as orientation, spacing, persistence, infilling, roughness, aperture, and weathering degree were defined by analyzing the cores and scan-line surveys according to ISRM (2007) suggested method.

The geophysical studies were performed by using the seismic refraction method in six lines to determine the dynamic Poisson's ratio (ν) of each geological unit. The dynamic Poisson's ratio values were calculated using the method proposed by Bowles (1988).

In order to determine rock mass parameters such as Hoek-Brown constants (mb, s, a), deformation modulus (Em), and uniaxial compressive strength (σcm), Hoek-Brown failure criterion suggested by Hoek et al. (2002) was used. The post-peak behavior of geological units upon tunnel excavation was determined with the help of method recommended by Cai et al. (2007). The most commonly utilized rock mass classification systems such as RMR, Q, and NATM were employed to characterize the geological units along the tunnel alignment and to conduct empirical support design. In this study, the latest version of the RMR system (Bieniawski, 1989) was considered. According to the RMR system, the geological units along the tunnel route were classified as poor and very poor rock masses. In terms of the Q system (Barton et al., 1974),

the geological units were classified as extremely poor and very poor rock masses. The main rock mass classes based on the NATM (Ö-NORM B2203, 1994) for the geological units were classified as B3/rolling and C1/rock bursting (Table 1).

In addition to this, the empirical tunnel support design (Table 1) was determined using the bolt length, bolt spacing and shotcrete thickness determination charts proposed by Lowson and Bieniawski (2013) and Barton (2002).

Table 1. RMR, Q, and NATM rock mass classifications and empirical tunnel support categories

Classification system	Subasi Ridge Formation	Cankurtaran Formation	Senkaya Ridge Formation	Kabakoy Formation
Basic RMR Adj. RMR Support	46.4 28.0/Poor Systematic rock bolts 6m long, spaced 0.7-0.9m and 250-300mm thick steel fibre/ wiremesh reinforced shotcrete (Sfr+B) in wall and crown	45.2 25.3/Poor Systematic rock bolts 6m long, spaced 0.7m and 250-300mm thick steel fibre/wire-mesh reinforced shotcrete (Sfr+B) in wall and crown	26.1 14.8/Very poor Cast concrete arch (CCA) or systematic rock bolts 6m long, spaced 0.5m and ≥300mm thick steel fibre/ wire-mesh reinforced shotcrete (Sfr+B) and steel ribs (RRS) in crown and wall	46.9 28.3/Poor Systematic rock bolts 6m long, spaced 0.9m and 250-300mm thick steel fibre reinforced shotcrete (Sfr+B) in wall and crown
Q Support	0.35/Very poor Crown: Systematic rock bolts 4m long, spaced 1.3-1.5m and 120-150mm thick steel fibre/wiremesh reinforced shotcrete (Sfr+B) Wall: Systematic rock bolts 3.5m long, spaced 1.5-1.7m and 90-120mm thick steel fibre reinforced shotcrete (Sfr+B)	0.49/Very poor Crown: Systematic rock bolts 4m long, spaced 1.5-1.7m and 90-120mm thick steel fibre reinforced shotcrete (Sfr+B) Wall: Systematic rock bolts 3.5m long, spaced 1.7-2.1m and 90-120mm thick steel fibre reinforced shotcrete (Sfr+B)	0.015/Extremely poor Cast concrete lining (CCA) or systematic rock bolts 4m long, spaced 1.0-1.2m and ≥250mm thick steel fibre/wire-mesh reinforced shotcrete (Sfr+B) and steel ribs (RRS) in crown and wall	0.30/Very poor Crown: Systematic rock bolts 4m long, spaced 1.3-1.5m and 120-150mm thick steel fibre reinforced shotcrete (Sfr+B) Wall: Systematic rock bolts 3.5m long, spaced 1.5-1.7m and 90-120mm thick steel fibre reinforced shotcrete (Sfr+B)

NATM	B3/Rolling	B3/Rolling	C1/Rock bursting	B3/Rolling
Support	Utilization of systematic support and local forepoles	Utilization of systematic support and local forepoles	Utilization of systematic support in roof and wall	Utilization of systematic support and local forepoles

4. Numerical Analyses and Proposed Tunnel Support Design

In order to determine the induced stresses, deformations, and developed plastic zones around the tunnel and to verify the results of the empirical methods, the FEM based computer software Phase2 v8.0 developed by Rocscience (2011) was used in the numerical analyses. An automatic mesh around the tunnel was generated and based on the elasto-plastic analysis, stresses and deformations were computed in this program. In order to analyze the deformations and tunnel stability and, to explore the concept of rock support interaction, a very simple model was used. Six-noded triangular finite elements were chosen in the mesh and finer zoning was applied around the excavation. The planned length of the double tube tunnel is 5.288 m and the excavation section is modified horse shoe-shaped with 12 m width and 9 m height. The excavation boundary of tunnel was generated considering its width and height in two stages as top heading and bench for the Subasi Ridge Formation, Cankurtaran Formation and Kabakoy Formation and, top heading, bench and invert for the Senkaya Ridge Formation according to construction procedure of the NATM (KGM, 2013). To simulate the tunnel excavation in all geotechnical units, four finite element models were generated using same tunnel geometry, mesh and different material properties. Hoek-Brown failure criterion was used to determine the plastic zones and yielded elements in the vicinity of tunnel. Material properties of the geological units used in the numerical analyses are given in Table 2.

The numerical analyses were performed in two steps as unsupported and supported cases for each geological unit considering groundwater condition and seismic effect. Taking into account the distance of the Black Sea Fault, the peak ground acceleration (PGA) value was determined to be 0.14 g using the Ulusay et al. (2004) attenuation relationship suggested for Turkey. Thus, a seismic loading of 0.14 g was applied into the analyze model. In the first step, following the examination of in-situ stress distributions, the yielded points, principal stress distributions, and induced displacements developed around the tunnel excavations were determined. Further, the maximum thickness of the plastic zones and total displacements were examined. In the second step, the performance of the empirical support design obtained from the RMR and Q classification systems were investigated using the same analyze model (Figure 3).

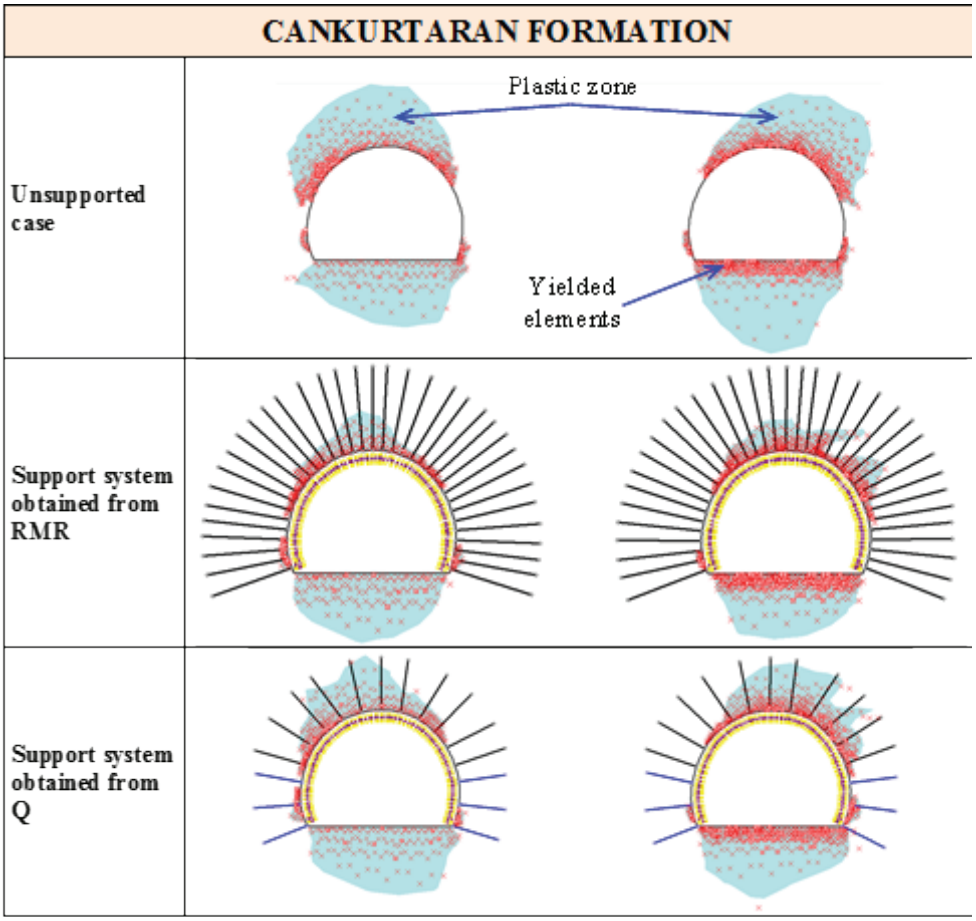

Figure 3. Numerical analyses showing the plastic zones developed in Cankurtaran Formation for unsupported and supported cases

It was concluded that the suggested empirical support designs are sufficient to provide the stability in the Subası Ridge Formation. It was observed that the support design suggested for the Cankurtaran Formation are not enough to reduce the maximum thickness of the plastic zones occurred in both roof and wall (Figure 3). On the other hand, the empirical support designs suggested by Q system were determined to be insufficient to reduce the plastic zones developed around the excavation boundary in the Senkaya Ridge Formation whereas all support designs were found to be applicable to prove the stability in the Kabakoy Formation.

Table 2. Material properties of the geological units for numerical analyses

Property	Subasi Ridge Formation	Cankurtaran Formation	Senkaya Ridge Formation	Kabakoy Formation
Elastic type	Isotropic	Isotropic	Isotropic	Isotropic
Rock mass strength (σ_{cm}, MPa)	14.00	11.66	1.44	19.99
Deformation modulus (E_m, GPa)	6.93	15.41	0.44	13.69
Poisson's ratio, υ	0.40	0.26	0.31	0.39
Material type	Plastic	Plastic	Plastic	Plastic
mi constant	7	8	7	25

m_b constant	0.93	2.06	0.34	5.78
s constant	0.0019	0.0147	0.0001	0.0105
a constant	0.509	0.502	0.561	0.503
m_{br} residual constant	0.47	0.59	0.31	1.83
s_r residual constant	0.00022	0.00030	0.00006	0.00029
a_r residual constant	0.533	0.527	0.573	0.528
Disturbance factor (D)	0	0	0	0
Dilation parameter	0	0	0	0
Vertical stress (σ_v, MPa)	2.30	12.80	1.82	2.97
Horizontal stress (σ_h, MPa)	1.53	4.50	0.82	1.90

The numerical analyses results indicate that the support designs suggested by the RMR and Q systems are not used safely to provide the stability of tunnel roofs in the Cankurtaran Formation having very poor quality under great field loading. Therefore, the support designs have to be revised for this formation. In order to determine the optimal support design, all support scenarios including different bolt and shotcrete patterns and adding steel ribs were analyzed. Finally, providing the RMR support design given in Table 1 remain same; when the uniaxial compressive strength of the shotcrete was increased from 20 MPa to 45 MPa and tensile strength from 3.1 MPa to 4.7 MPa considering the tunnel specification of the KGM (2013), the extent of the plastic zones reduced to zero (Figure 4 and Table 3).

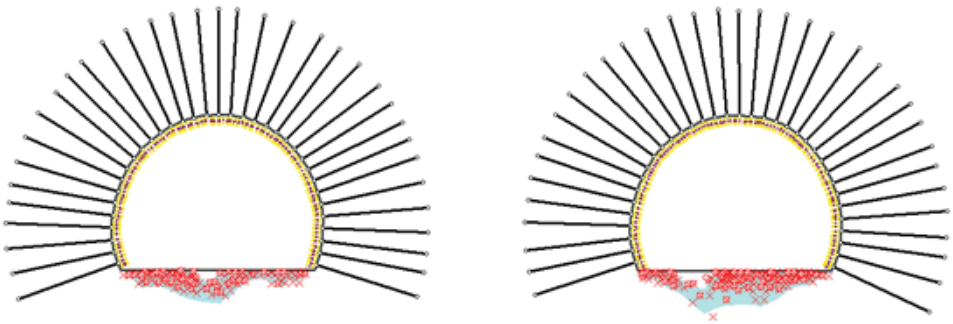

Figure 4. Plastic zones and yielded elements developed after application of the suggested support designs in the Cankurtaran Formation

Table 3. Stresses, displacements and the maximum thickness of plastic zones after revised support installation in the Cankurtaran Formation

		Left tube	Right tube
Roof	σ_1 (MPa)	7.35	6.30
	σ_3 (MPa)	1.70	0.90
Floor	σ_1 (MPa)	1.05	0.00
	σ_3 (MPa)	0.10	0.10
Left wall	σ_1 (MPa)	3.15	4.20
	σ_3 (MPa)	0.50	0.50
Right wall	σ_1 (MPa)	4.20	3.15
	σ_3 (MPa)	0.50	0.50
	T_{pl} (m)	0.00	0.00
	U_t (m)	0.0147	

σ_1 : Maximum principle stress (MPa)
σ_3 : Minimum principle stress (MPa)
U_t : Maximum total displacement (m)
T_{pl} : Maximum thickness of plastic zone (m)

5. Results

In this study, preliminary support design of the Cankurtaran tunnel was investigated. The rock masses along the tunnel alignment were characterized by means of the RMR, Q and NATM rock mass classification systems. The rock masses were classified as ranging from extremely poor quality rock mass to poor quality rock mass. In order to estimate the appropriate support requirements related to geotechnical rock mass parameters for the tunnel, these classification systems were also employed. FEM method was undertaken to check the validity of the empirical preliminary tunnel support requirements. Phase2 software was used to determine the induced stresses, maximum total displacements, and thickness of plastic zones developed around the rock masses surrounding the tunnel. According to results, the empirical support design recommended for the Cankurtaran Formation was not enough to reduce the maximum thickness of the plastic zones occurred in roofs. Therefore, a new support design was recommended using the numerical models considering the all possible support scenarios. When the strengthened shotcrete having an optimum strength value of 45 MPa was applied into the shotcrete liner pattern suggested by the RMR system, the deformations were stopped and the maximum thickness of the plastic zones were decreased to zero.

Consequently, the numerical analyses proved that the empirical support designs did not give the realistic solutions in very poor rock masses under great in-situ rock stresses. Therefore, it is suggested that the validity of the support design recommended by the empirical methods should be controlled prior to excavation phase using the numerical analyses and numerical models should be checked with the monitoring systems during the construction of a tunnel. Further, the rock masses in portals and fault zones should be reinforced with heavier supports in the form of steel sets or cast concrete arches.

References

Barton, N.R., Lien, R., Lunde, J., 1974. Engineering classification of rock masses for the design of tunnel support. Rock. Mech., 4, 189-239.

Barton, N., 2002. Some new Q-value correlations to assist in site characterization and tunnel design. Int. J. Rock Mech. Min. Sci., 39(1), 185-216.

Bieniawski, Z.T., 1989. Engineering Rock Mass Classifications. Wiley, New York, 251 p.

Bowles, J.E., 1988. Foundation analysis and design. McGraw-Hill Book Company, New York.

Cai, M., Kaiser, P.K., Tasaka, Y., Minami, M., 2007. Determination of residual strength parameters of jointed rock masses using the GSI system. Int. J. Rock Mech. Min. Sci., 4(2), 247-265.

Capkinoglu, S., 1981. Geology of the district between Borcka and Cavuslu (Hopa). MSc. Thesis, Karadeniz Technical University.

Deere, D.U., 1964. Technical description of rock cores for engineering purposed. Rock Mech. Rock Eng., 1, 17-22.

Guven, I.H., 1993. 1:250000-scaled geology and compilation of the Eastern Pontide. General Directorate of Mineral Research and Exploration (MTA) of Turkey, Ankara (unpublished).

Hoek, E., Carranza-Torres C., Corkum, B., 2002. Hoek-Brown failure criterion-2002 edition, NARMS-TAC2002, Mining Innovation and Technology, Toronto, Canada, 267-273 pp.

ISRM, 2007. The complete ISRM suggested methods for rock characterization, testing and monitoring: 1974-2006, International Society of Rock Mechanics Turkish National Group, Ankara, Turkey, 628 p.

Kaya, A., 2012. The geotechnical investigation of the Cankurtaran (Hopa-Artvin) tunnel alignment and surrounding area. Ph.D. Thesis, Karadeniz Technical University.

Kaya, A., Bulut, F., 2013. Stability analyses of tunnels excavated in weak rock masses using empirical and numerical methods, Journal of Geological Engineering, 37(2), 103-116.

KGM, 2013. Specification for highway works (in Turkish), Turkish Ministry of Public Works, General Directorate of Highways, Ankara.

Lowson, A.R., Bieniawski, Z.T., 2013. Critical assessment of RMR based tunnel design practices: a practical engineer's approach, Rapid Excavation and Tunneling Conference, Washington D.C., USA.

Ö-NORM B2203, 1994. Untertagebauarbeiten werkvertragsnorm, Österreichischer Normen, Österreich.

Priest, S.D., Hudson, J.A., 1976. Discontinuity spacing in rock. Int. J. Rock Mech. Min. Sci. Geo. Abs., 13, 135-148.

Rocscience, 2011. Phase2 v8.0 finite element analysis for excavations and slopes, Rocscience Inc., Toronto, Ontario, Canada.

Ulusay, R., Tuncay, E., Sonmez, H., Gokceoglu, C., 2004. An attenuation relationship based on Turkish strong motion data and iso-acceleration map of Turkey. Eng. Geo., 74(3–4), 265-291.

Makale Gönderim Tarihi: 10.07.2016
Yayına Kabul Tarihi: 28.08.2016

Modelling of Underground Natural Gas Storage Openings in the Basin of Tuz Gölü Lake with FEM

Ümit Güney [1], İrfan Celal Engin [2]*
[1] *Eskişehir Osmangazi University, Mining Engineering Department, Eskişehir*
[2] *Afyon Kocatepe University, Mining Engineering Department, Afyonkarahisar*
* *Corresponding Author: icengin@hotmail.com*

Abstract
The need to energy is increasing in the world with the increasing of industrialization day by day. In this context there is a growing need for energy obtained from natural gas. In Turkey, parallel to the world the demand for natural gas is also increasing. Annual natural gas consumption in Turkey is about 50 billion cubic meters. Distribution of Turkey's natural gas consumption according to usage areas is as follows; 53% in electrical energy, 25% in industry, 22% in residential use. These demands rates are varying according to different times of the year. Moreover, due to political crisis, differences in the gas flow may occur. It is possible to become inadequate to meet immediate demand for these differences. Creation of underground natural gas storage is considered as a solution to eliminate this risk. While, the world storage volume is 380.4 billion cubic meters, Turkey has one store with 2.6 billion cubic meters capacity. It is also planned for storage capacity as 10% of the demand in Turkey. In this study, the stress around natural gas storage underground openings, designed by BOTAŞ in the Basin of Tuz Gölü Lake, and the resulting deformation were investigated. For this purpose, Rocscience RS2 (Phase2) using finite element analysis was performed. Analysis were carried out for a single opening and also multiple neighbor caverns. Working gas pressures are suggested for each modelled situations.

Keywords: Tunneling, Rock mass classification, Support design, FEM.

1. Introduction

Energy requirement is increasing along with industrial growth worldwide. Electrical energy is at the top of these energy needs. A majority as 37.8% of electricity production are supplied by the natural gas conversion plants in our country according to 2015 data (MENR, 2016). At the same time, natural gas usage in the different branches of industry and housing is quite common. This situation increases the demand of natural gas day by day.

Although dependence on natural gas is so much natural gas production in our country is quite low. It means that the majority of this gas is imported from abroad. The difficulties may be encountered some time due to a variety of reasons in meeting the natural gas needs. The main causes are as follows: Failing of the gas provider countries in meeting the natural gas demand of our country, political reasons and fluctuations in demand for natural gas. Demand for natural gas is increased, especially with the increased need for heating in winter. But the summer demand in the residential use of natural gas fairly decreases because natural gas usage for heating is not needed. Natural gas consumed in our country is used as 53% percentage in the production of electricity and as 22% in residential housing and as 25% in the energy production for industry as shown in Figure 1 (Özarslan et al., 2007). When we look at the amount of natural gas consumed in housing at summer and winter months the ratio between the months is seen as a serious fluctuations.

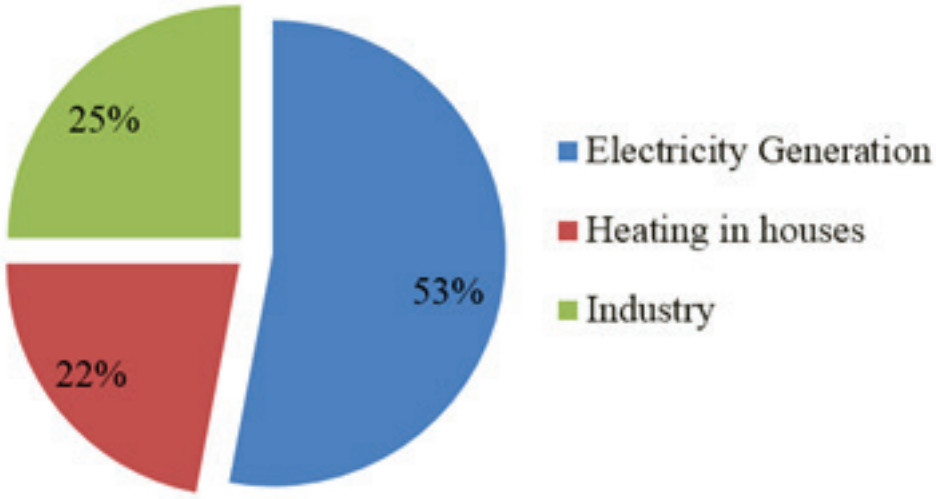

Figure 1. The purposes of the natural gas usage in Turkey

Gas quantity to be stored in Turkey and Europe, respectively, should be 10% and 20% based on the amount of total usage. When we look at these figures and consider the increased supply, the gas quantity to be stored is inadequate by the ratio 2.1% according to the laws of Turkey and by 4.2% of Europe today. In 2030 this ratio is expected to be insufficient by 4.9% as compared to Turkey and as 9.8% to Europe (Dülger, 2013). Therefore, it is increasing the attention paid to the storage of natural gas.

Underground storage is safer as well as more economical according to the surface storage tanks. Underground reservoirs can hold much more gas on site according to the surface tanks. Underground reservoirs also vary among themselves. One of the ideal solutions is openings which are formed by solution mining in rock salt. Gas can be stored safely in these spaces. In addition,

an impermeable reservoir can also be provided with the self-repair of cracks that may exist in the salt (Özarslan et al., 2007). Openings can maintain their stability without artificial supports (Özarslan et al., 2007). Natural gas storage in rock salt is opened with the aid of solution mining. Dissolution of the salt is provided by giving fresh water to the drill hole at the appropriate depth. Large underground cavities can be opened in this way. These opened cavities is important to have a desired geometry. In particular, the uncontrolled growth of the openings upwardly is undesired. Substances such as oil, helium gas and etc. is sent into the drilling hole to prevent the uncontrolled dissolution. These substances should remain above the water and also not react with the water, salts and natural gas.

The Tuz Gölü salt formation is folded up to an elongated narrow salt wall by post-sedimentary halokinetic processes. Based on seismic data, the salt body exhibits a rather complex and irregular subsurface topography with rather steep dipping flanks. Within the presumed cavern area, the top of salt formation is expected in depth between 595 m and 1,085 m. Table 1 presents general geological and lithological information about the profile of the field (Onal, 2013).

Table 1. Stratigraphic preconditions of the field (Onal, 2013)

Stratigraphic formation / unit or subunit	Estimated thickness range (m)	General Lithology
Cihanbeyli to Kochisar fm.	640 – 1.080	Shale, marlstone, conglomerates and limestones
Caprock	65 – 95*	Anhydrite occasionally with thin intercalations of clay and/or carbonates
Salt	> 1.000	Rock salt with an average of about 7 to 11% of insolubles (mostly anhydrite), locally up to 26%

The main factors to be considered in the design of the opening; depth, primary stresses, opening geometry, short and long-lasting mechanical properties of the rock salt and inner gas pressure conditions. The general approach to internal gas pressure is followed as, 30% of the maximum principal stress is taken as the smallest internal pressure, and 80-85% of the maximum principal stress is taken as the greatest internal pressure. Low minimum internal pressure will cause failure in protecting the stability of the opening but excessive amount will result as uneconomical solution. The higher maximum internal pressure values can cause hydraulic fracturing of rock salt and formation of fissures and gas leaking. In contrast, the low maximum internal pressure will also result as uneconomical solution. In addition, the distance between the two openings is an essential parameter to be considered if there are other openings in the planned study area (Özarslan et al., 2007).

RS2 (Phase2) finite element program produced by the Rocscience company is used in the modelling. Mohr - Coulomb failure criterion was used in the program. The geometry of the gas reservoir was introduced into the software. The mechanical properties of the formation and the location of the gas reservoir is defined first. Then stress-deformation calculation for each node is made by creating the mesh in the software. Different internal pressures and the effects of neighboring natural gas storage were examined in the calculations.

2. Effective Parameters in Design of Natural Gas Storages Opened in Rock Salt

2.1. Depth and Principle Stresses

The storage is located at 1150 meters depth in this study. The unit weight of the cover layer in the region where underground storage exists was taken as 0.025 MN/m^3 and unit weight of rock salt was taken as 0.021 MN/m^3. Average unit weight can be taken as 0.024 MN/m^3. It was considered that the primary stress is due to gravity, and was calculated as about 27 MPa.

2.2. The Geometry of the Opening

The diameter of the opening, which is opened in rock salt is up to 64 meters and the height is 300 meters geometric form of the opening is given in Figure 2. Depth from the surface of the natural gas storage is taken as 1150 m. The area of opening is approximately 15.300 m^2 and the volume is 675.000 m^3. It is intended to establish the closest model to the real opening with that planned geometry.

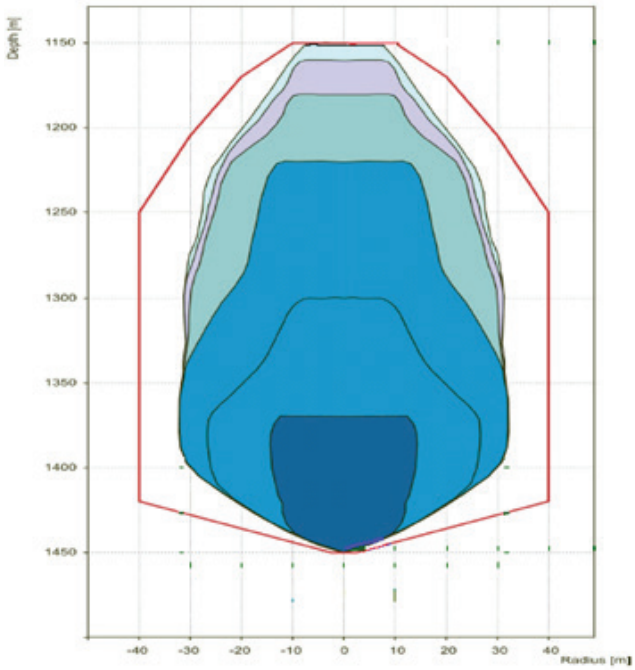

Figure 2. Geometric form of the natural gas storage opening used in the modeling study (Dülger, 2013)

2.3. Internal Gas Pressure

Internal gas pressure, is one of the most important parameters in order to maintain the stability of the natural gas storage in rock salt. The minimum gas pressure gives the minimum internal gas pressure value required to keep the reservoir stable. This value is approximately between 25-30% of the principle stress (Özarslan et al., 2007). The maximum gas pressure gives the highest value of internal gas pressure allowed in the gas storage. Maximum gas pressure value is between 75-80% of the principle stress. If the maximum gas pressure exceeds these values hydraulic fracturing may act on the wall of the opening (Özarslan et al., 2007). When these values are considered, the minimum gas pressure should be between 6.75 and 8.1 MPa, the maximum gas pressure should be in the range of 20.25 to 21.6 MPa.

2.4. Mechanical Properties of Rock Salt

The mechanical properties of rock salt, where the gas storage is opened, is an effective parameter to remain stable. The mechanical properties of the formation used in the modelling are given in Table 1.

2.5. Distance Between two Adjacent Openings

Distance between the gas storage openings in other words pillar thickness is important for the stability of the system. Induced stress zone created by one of the opening should not affect the other neighboring storage. If there is less distance between the openings, induced stress zones will coincide with each other, and therefore the stability of the reservoir will be affected negatively. In contrast, in an excess of the distance between the openings storage areas cannot be used effectively. Such factors should be considered and optimal distance between stores should be left. In this study, models were created for 150 m and 300 m distances between two adjacent openings.

3. Modelling of Underground Natural Gas Storage Openings using Rocscience RS2 Finite Element Method

In the modeling study is performed using the finite element program RS2 (Phase2) version 9.0 produced by the company Rocscience. Stress conditions was taken as hydrostatic and maximum stress component was considered as the stress created by overburden. Modeling was conducted in the specified elastic conditions. The values adopted to modelling is given in Table 2 (Özşen, 2009). Mohr - Coulomb failure criteria was selected and type of material was taken as plastic. Density of the overburden was taken as 0.023 MN/m^3

Table 2. The parameter values used in modelling with finite element method.

Parameter	Unit	Rock Salt
Unit Weight	MN/m^3	0.021
Cohesion	MPa	4.8
Angle of Internal Friction	Degree	61
UCS	MPa	27.8
Poisson ratio	-	0.11
Young's Modulus	GPa	2.29
Tensile Strength	MPa	2.69

The storage openings are planned to be built at 1150 m depth and maximum principle stress calculated from gravity is 27 MPa at that depth. The situations that are used in different modelling scenarios are given in Table 3.

Table 3. Different planned situations used in the models

Model No	Distance Between Openings (m)	Internal Gas Pressure (MPa)
1	0 (Single Opening)	0
2	0 (Single Opening)	8
3	0 (Single Opening)	22
4	150	0
5	150	8
6	150	22
7	300	0
8	300	8
9	300	22

3.1. Results of the Modelling Study

Stress distributions and total displacements values were calculated for ten different situations given in Table 3. Distribution of the maximum principle stress and total displacement around the opening is given at Figure 3 for internal pressure equal to zero. Internal pressure of the storage is selected as 0 MPa, 8 MPa and 22 MPa in modelling. Total displacement around the opening is given in Figure 4 for single opening. Modelling study was performed for the opening formed at 150 m and 300 m distances (Figure 5, Figure 6).

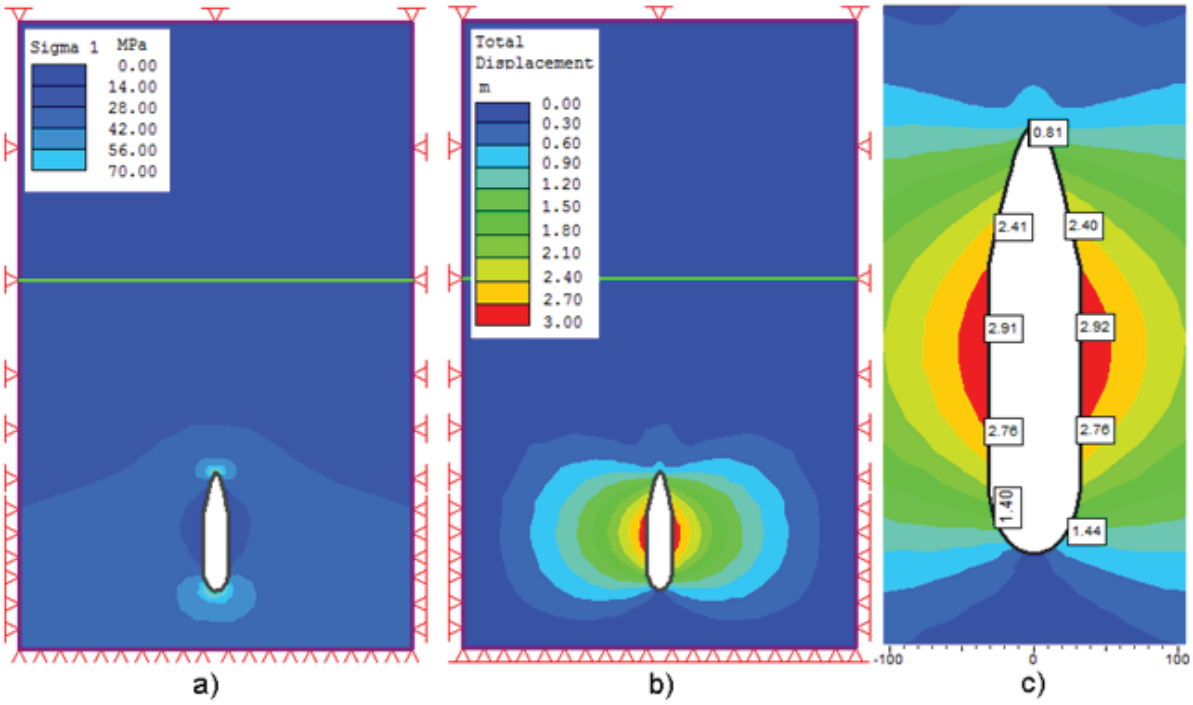

Figure 3. Maximum principle stress (a) total displacement (b) distribution around the opening, and total displacement values at different locations

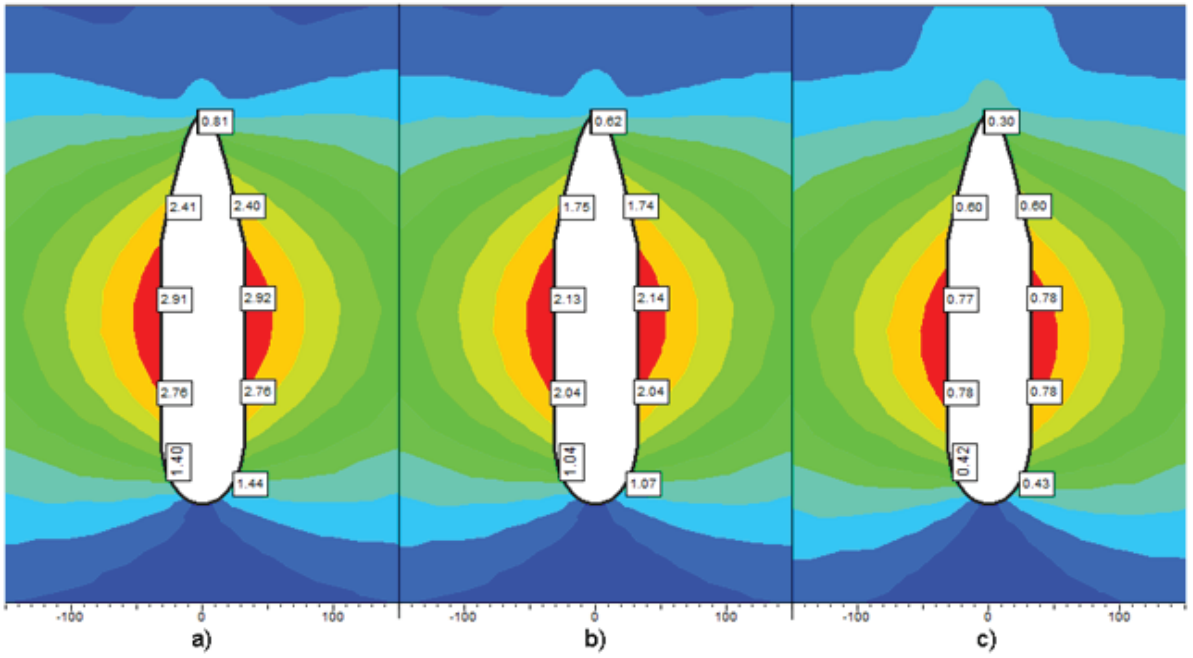

Figure 4. Total displacement values at different locations for internal pressure 0 MPa (a), 8 MPa (b), and 22 MPa (c) in single opening situation.

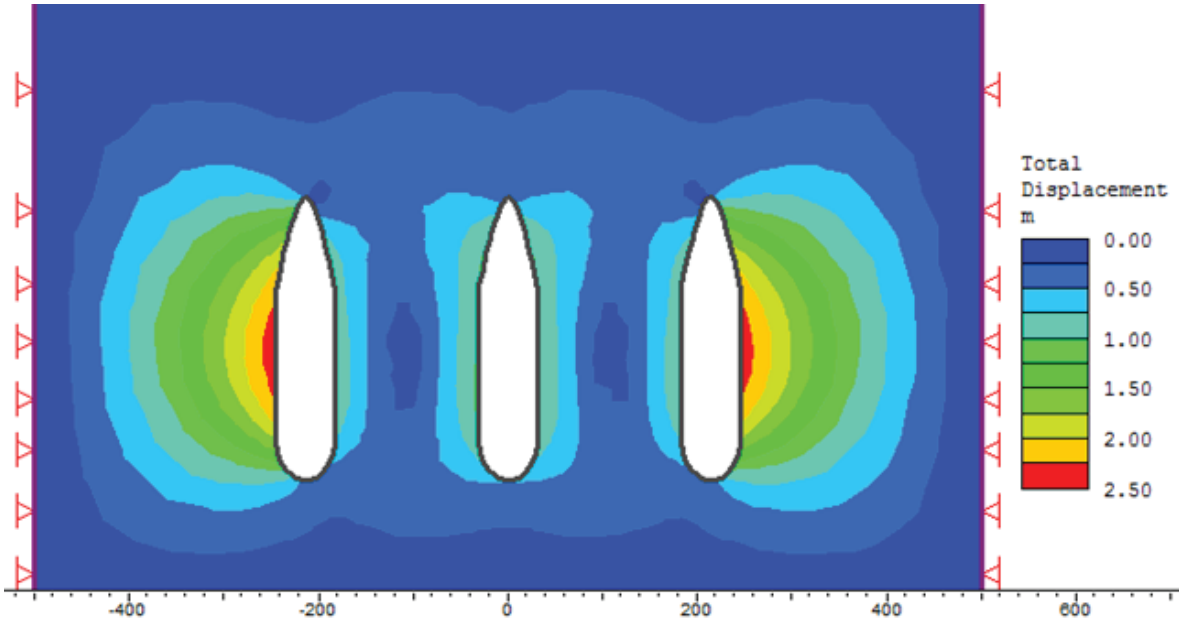

Figure 5. Total displacement values for the openings within 150 m and 0 MPa internal pressure.

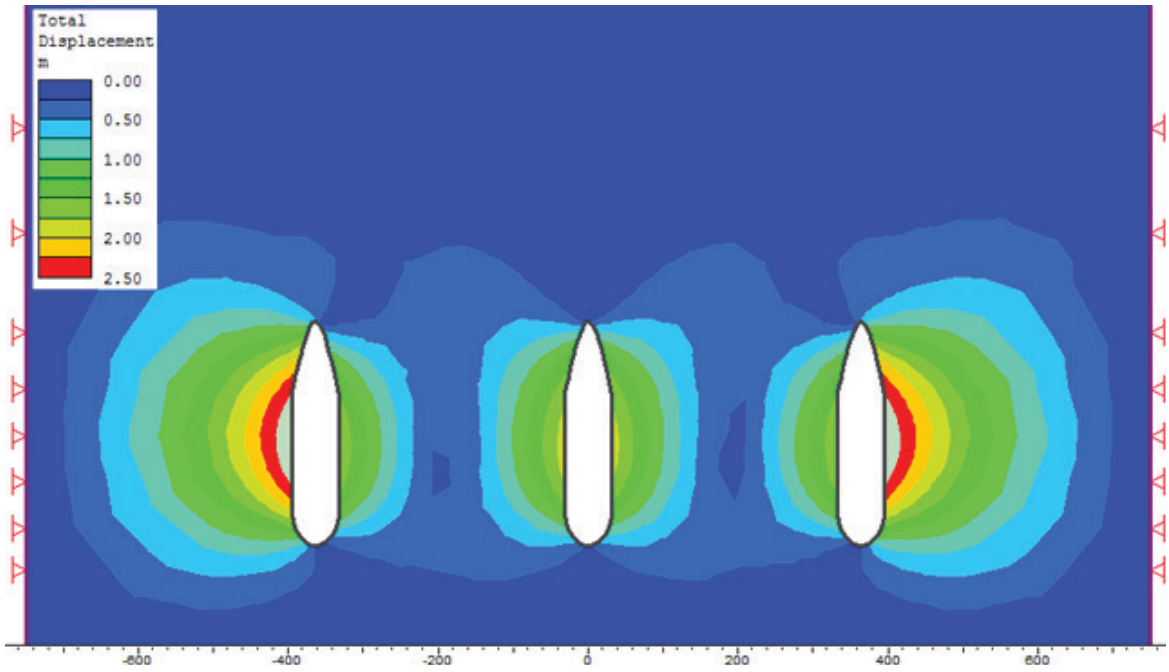

Figure 6. Total displacement values for the openings within 300 m and 0 MPa internal pressure.

In modeling with finite elements, the closer the openings are, the less the deformation between them is. According to widely accepted view, when the natural gas reservoirs approach each other, the deformation increases. But the opposite is true in the model here. The reason for this is that deformations are taken as vectors. As shown in Figure 7, the vectors are damped because of the opposite directions, and therefore displacements decrease as the openings become closer to each other. When these explanations are taken into account, when the displacement is solved by the finite element, the distance between the underground natural gas storages cannot be decided. The best decision mechanism that can be applied here will be the primary stresses when the primary tensile strengths of the underground natural gas reservoirs are not within the confluence area, they should be considered as providing adequate spacing.

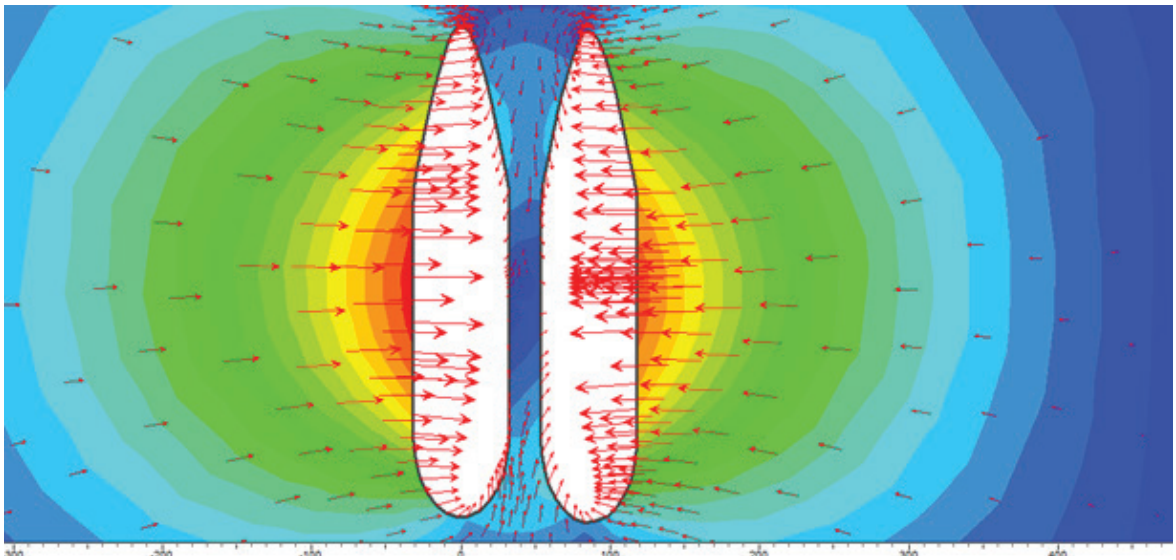

Figure 7. The displacement vectors of the two underground natural gas reservoirs, which have been reduced to extreme distances between them.

Figure 8 and Figure 9 show the state of the primary stresses as the distance between the storages changes according to the internal pressure being 0 MPa. In Figure 2, when the primary stresses on the two sides of the 1st and 3rd storages from left to the right are examined, it is observed that the differences reach about 10 MPa. It is observed that for the storage with a distance of 300 m between them, these differences reach to approximately 4 MPa. Figures 10-13 show primary stresses for internal pressures of 8 and 22 MPa. For these values taken as operating pressures, the primary stress fields can be determined in the same way. In this way, the distances between the storages in the model are determined so that the primary stresses on the two side surfaces of the first and third reservoirs are close to each other so that the tension fields of the storages are not influenced by each other.

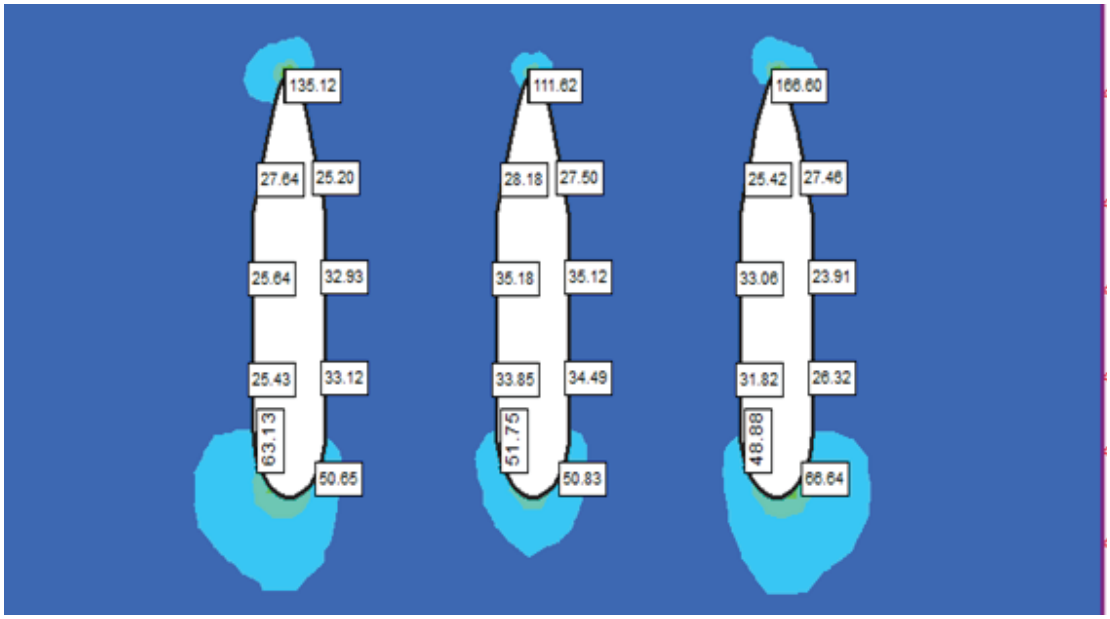

Figure 8. 0 MPa internal pressure and distance between openings 150 meters.

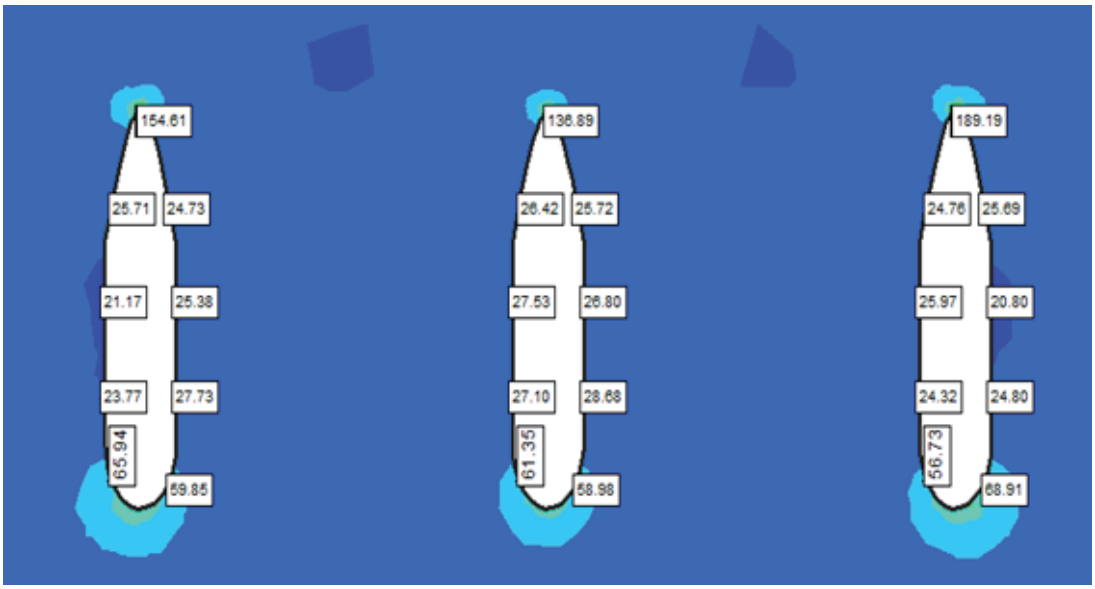

Figure 9. 0 MPa internal pressure and distance between openings 300 meters.

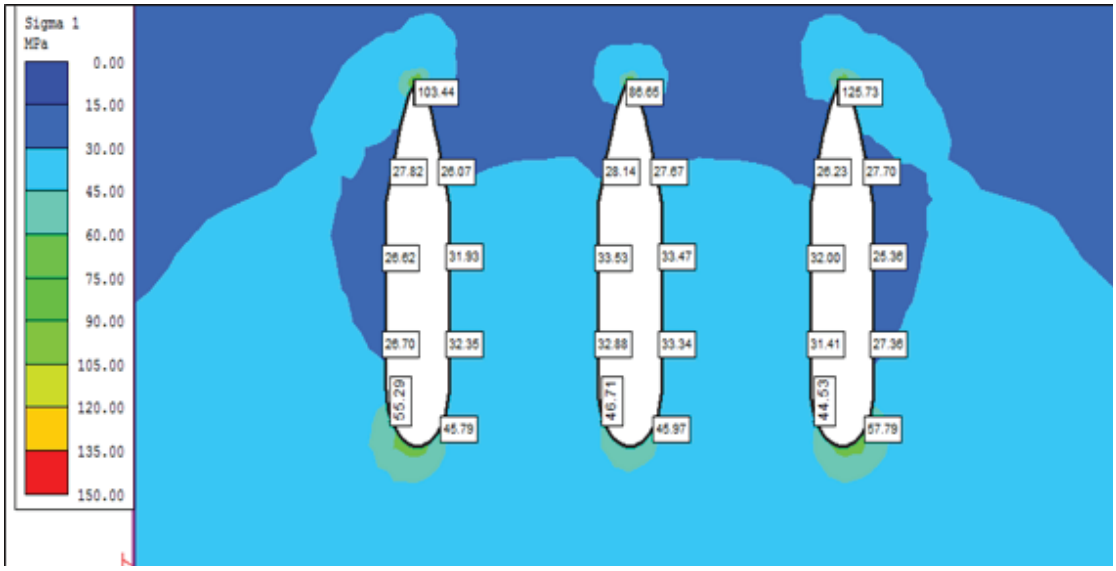

Figure 10. 8 MPa internal pressure and distance between openings 150 meters

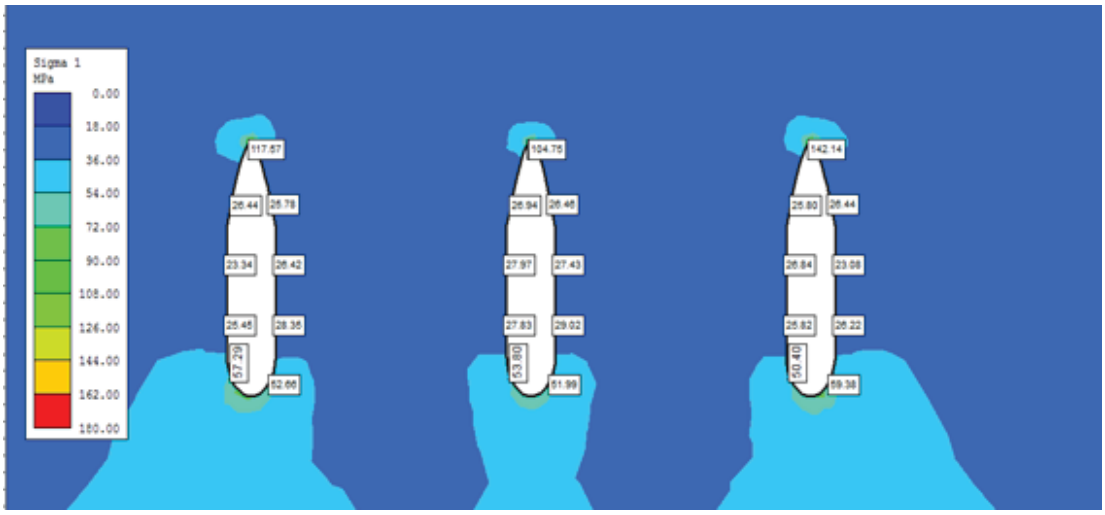

Figure 11. 8 MPa internal pressure and distance between openings 300 meters.

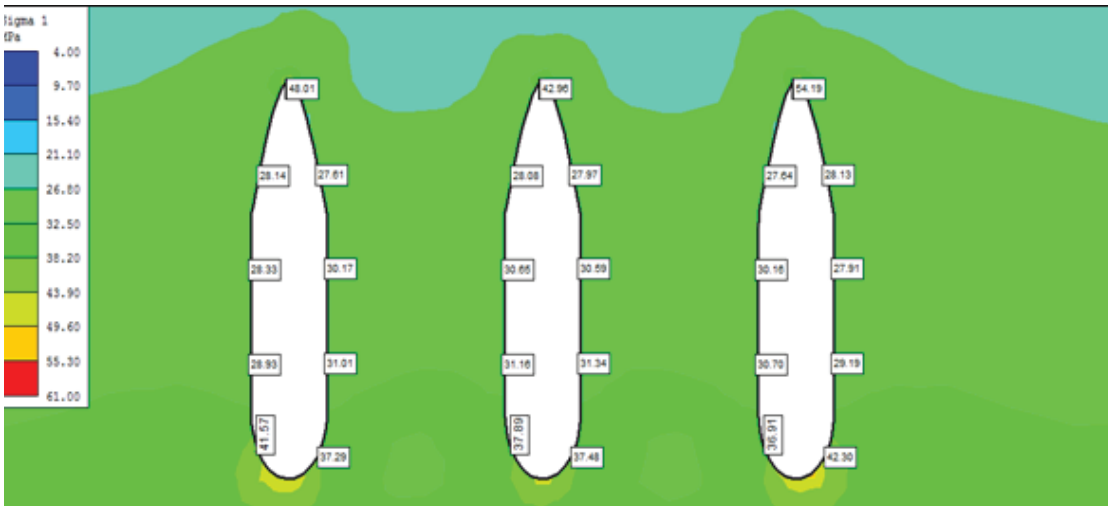

Figure 12. 22 MPa internal pressure and distance between openings 150 meters.

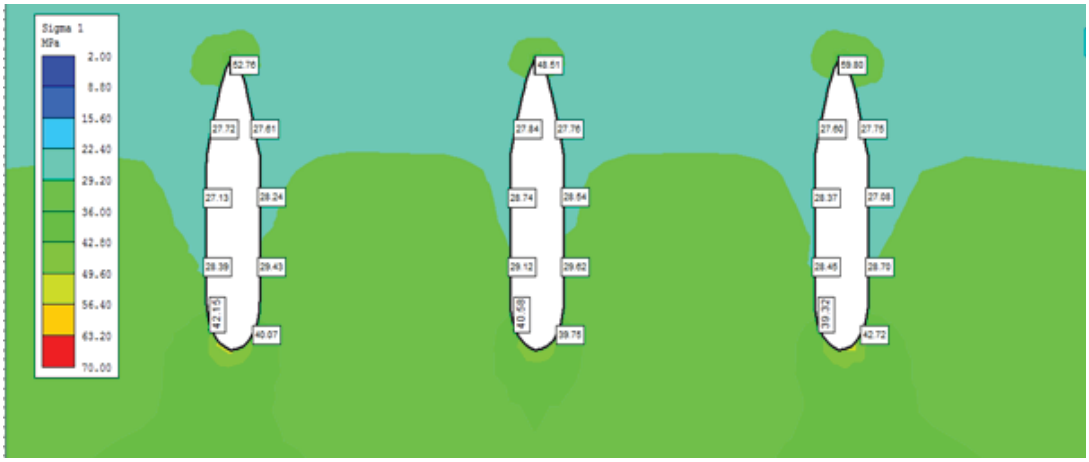

Figure 13. 22 MPa internal pressure and distance between openings 300 meters.

The relation between the stress differences observed at the side wall of the openings and the distance between the openings is given in Figure 14. When the internal pressure is increased, the pressure differentials on the lateral surfaces will decrease.

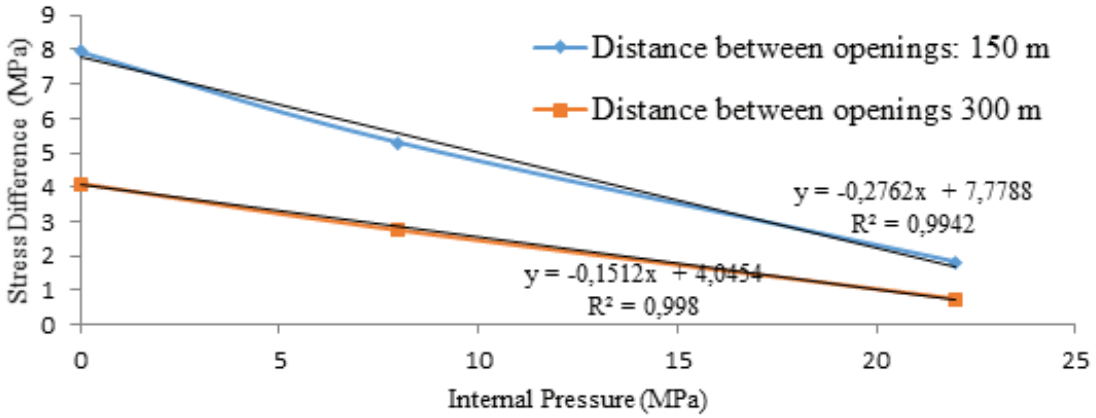

Figure 14. Variation of the stress difference between the lateral surfaces by the internal pressure values for the distances between the different openings

4. Results and Conclusion

The study of design parameters of gas storages was performed using the numerical analysis based on the finite element modeling (FEM), using a commercial software RS2 9.0 by RocScience. The analysis included geometrical parameters of the cavern i.e. shape and size, depth, specific gravity of overburden rocks and thus the in-situ stresses, ratio of lateral stress, elastic properties of rock, and strength of rock salt. The results of the study can be summarized in Table 4.

Table 4: Results of gas storage opening numerical analyses

Modelling Scenarios	Maximum Stress, σz MPa	Maximum Total Displacement, m	Maximum Shear Strain	Maximum Volumetric Strain
1	55.23	2.92	0.057	0.10
2	47.05	2.14	0.041	0.07
3	33.16	0.78	0.012	0.02
4	43.25	2.37	0.030	0.06
5	38.37	1.73	0.021	0.04
6	33.08	0.66	0.006	0.01
7	46.72	2.72	0.034	0.07
8	40.88	1.99	0.024	0.05
9	33.13	0.74	0.007	0.01

Maximum displacement often occurs on the sidewalls where the long unsupported span is located. Maximum displacements of less than 2% of diameter is often considered as acceptable for stability of underground structures, and can be used as a general measure of acceptability of wall displacement for given cavern sizes, shapes, and depth. The models in this study provided suitable results for this issue and in most cases, this requirement was met.

Study of loading and unloading of the cavern by injection/storage, and withdrawal of the gas during the life cycle of the caverns during the operation and its impact on the displacements and cavern stability has to be investigated.

Apart from this work, the formation of three-dimensional model will give different angles of stress and strain components. Furthermore, to determine the mechanical properties of rock salt, the changes that occur over time should also be considered. Also, the modeling must be done in different geometries.

References

Dülger M. G., 2013. Tuz Gölü Doğalgaz Yeraltı Depolama Projesi, Doğal Gaz Yeraltı Depolama Daire Başkanlığı, 7. Taşıtanlar Forumu, Sunum, 25 Nisan 2013, 30 s.

Ministry of Energy and Natural Resources (MENR) (2016, July 19). Retrieved from http://www.enerji.gov.tr/tr-TR/Sayfalar/Elektrik

Onal, E., 2013. Stability Analyses of Differently Shaped Salt Caverns For Underground Natural Gas Storage, The Pennsylvania State University The Graduate School College Of Earth And Mineral Sciences, May 2013, 145 p.

Özarslan, A., Geniş, M., Bilir, E., 2007. Doğal Gaz Depolama Amaçlı Yeraltı Tuz Çözelti Açıklıklarının Farklı İşletme Koşulları Altında Duraylılığın İncelenmesi. Tübitak Projesi, TÜBİTAK MAG Proje 104M132, 117 s.

Özşen, H., 2009. Kaya Tuzuna Ait Kısa ve Uzun Dönemli Mekanik Özelliklerin Belirlenmesi ve Matematiksel Modellenmesi. Doktora Tezi, Selçuk Üniversitesi Fen Bilimleri Enstitüsü, 315 s.

Makale Gönderim Tarihi: 21.07.2016
Yayına Kabul Tarihi: 11.08.2016

Investigation of Top Coal Cavability and Roof Behavior by Ground Response Curves

İbrahim Ferid Öge [1]*
[1] *Muğla Sıtkı Koçman University, Department of Mining Engineering*
**Corresponding Author: feridoge@mu.edu.tr*

Abstract
Longwall top coal caving mines are commonly operated at a depth of 100-400m in Soma Coal Basin located at western part of Turkey. Mining activities will move to a depth greater than 700m in the near future together with the progress in the mine plan. 800m deep and 16m thick coal seam is considered in this study and cavability character of top coal and roof behavior were examined by numerical modelling incorporated to ground response curves in addition to empirical approach. 400m and 800m deep mining activities are compared by utilizing vertical stress distributions, displacements, and ground response curves representing each case.

Keywords: Longwall top coal caving (LTCC), Numerical Modeling, Coal Mining, Cavability Index, Ground Response Curve.

1. Introduction

There are a variety of thick coal seam extraction methods such as multi slice longwall method, blasting gallery method. Among them, longwall top coal caving (LTCC) method gains the highest attention due to low development work per produced coal. Turkish top coal caving experience lies back to early 80s and new thick seam coal mines are being proposed and some of them have initiated production (Doktan and İnci, 1986;1987; Başarır et al., 2015).

Top coal caving method can simply be explained as drawing the coal overlying the powered shield (top coal) at rear canopy flipper of the shield while a conventional longwall production is limited to face cutting. LTCC requires elaborateness in face operations to have a successful production performance. The method provides increased productivity, less development length per produced coal tonnage. When LTCC is compared to other thick coal seam production methods like multi-slice longwall method, it is superior from technical and economical point of view (Vakili and Hebblewhite, 2010; Alehossein and Poulsen, 2010).

Typical single-pass LTCC applications generally work in a coal seam thickness up to around 12m. In coal seams having greater thickness, multi-pass LTCC can be applied in order to achieve better recovery (Başarır, 2015; Aksoy et al. 2015;2016). Still, questions on cavability tendency of the top coal remains hard to be answered accurately. Findings of a top coal cavability assessment may help decisioning on production fashion being either multi slice or single pass LTCC for a greenfield project as being a challenging rock mechanics problem. One of the other challenging part of the problem is the assessment to be conducted for a proposed operation of LTCC under great depth since worldwide top coal caving experiences are generally restricted up to 600m and deeper top coal caving experiences are rare over the world and absent in Turkey.

2. Soma Lignite Coal Basin

Soma lignite coal basin is located at Soma province in Manisa / Turkey. An open cast mine is under operation in the northern region of the basin where the coal seam lies at shallow depth. In neighborhood, underground coal mines are under operation at a depth range of 150-400m. New underground coal mines are being projected having greater mining depth from 700m to 1200m which are owned by government and private companies.

2.1. Geology and Rock Mass Properties

Main coal seam named as KM2 has economic significance and being extracted in the basin. Thickness of KM2 varies between 5 to 30m along the basin. Quality and calorific value of the coal decreases from top to bottom. Around mid-level of the coal seam, clay-claystone content starts to increase and strength of coal and structural quality decreases accordingly. KM2 is underlain by M1 geological unit consisting of poorly cemented clayey conglomerate and sandstones. M1 unit can be encountered having higher clay content in several regions of the basin which is prone to operational problems. In the northern basin, there are zones where coal seam inclination is 25° and it drops to nearly horizontal at southern and south-western regions. It is noticeable that in tectonically affected regions the seam has steep inclinations even though general trend is near horizontal. M2 unit consists of marl and overlies KM2 horizon with a thickness of 30 to 70m and exhibit massive structure with widely spaced beddings and sub-vertical calcite filled joints. A three-meter-thick zone (considered as immediate roof) of M2, overlies the KM2 coal, is structurally more deformed when it is compared to the upper zones of M2. Overburden lying on M2 unit is relatively weaker than M2 unit. Upper zones of overburden mostly consist of claystone, marl, sandstone, pebblestone, limestone intercalations. One of the main character

is strong tectonic disturbance over the basin and drastic changes on the structural quality of the rock mass which can be frequently observed in short intervals.

Input parameters are based on laboratory tests and borehole investigations, and final findings are reported. The parameters to be used in the analyses are given below (Table 2). Residual state strength parameters were calculated by assigning rock mass a GSI value for residual state (Cai et al., 2007) and Generalized Hoek-Brown parameters were calculated as described in (Hoek et al., 2002;2013; Marinos, 2014):

Table 2. Rock mechanics parameters of the geological units

	E_{rm} (GPa)	c_p (MPa)	φ_p(°)	σ_{tp} (MPa)	c_r (MPa)	φ_r(°)	σ_{tp} (MPa)
overburden	0.7	0.4	38	0.08	0.2	34	0.04
	E_{rm} (GPa)	σ_{ci} (MPa)	GSI_{peak}	GSI_{res}	mi	$m_{b,peak}$	$m_{b,res}$
M2 Marl	12.325	70	80	28	25	12.239	1.911
M2 Marl immediate roof	7.28	70	60	23	25	5.991	1.598
KM2 Upper coal zone	2.449	30	75	26	10	4.095	0.712
KM2 Middle coal zone	2.449	30	70	26	10	3.425	0.712
KM2 Bottom coal zone	0.319	10	55	20	10	2.005	0.574
M1 Clayey	1.225	15	55	24	10	2.005	0.663
M1 Conglomerate	0.798	25	40	23	12	1.408	0.767

2.2. Longwall Top Coal Caving Method in Soma Basin

Semi-mechanized and mechanized longwall faces are present in northern Soma basin. In northern Soma coal basin, Isiklar colliery is being operated in 20-25° steep coal seam with horizontal longwall faces, retreating parallel to the strike of the coal at 150-300m depth. Establishing horizontal longwall faces in 20-22m thick and steep coal seam, restrains the face length to 60m. Top coal thickness is adjusted to be in the range of 16-18m in vertical extent. Due to short face length, competent main roof and shallow depth, there is a potential of gathering poor recovery of top coal and standing of main roof were encountered especially for the upper production panels. Production sequence starts from the uppermost slice. Especially in lower consecutive panels, complete caving and drawing (recovery >90%) of the top coal was achieved by the help of pre-fracturing blasting and progressive damage of main roof, successfully. Main roof caving tendency increased and became no longer a problem for further production due to previous production induced damage to the roof. Strong mine induced deformation and stress re-distribution can be observed.

Other coal mines neighboring to the shallow ones, operating in near-horizontal thick coal seams (up to 30m thickness) prefer production of upper most coal slice in conventional longwall method. Operators aim to cave the main roof by conventional longwall mining of the uppermost

slice. The rest of the coal seam can be produced in one or two slices of semi-mechanized and mechanized LTCC (Yılmaz et al., 2013; Aksoy et al., 2016) with varied face lengths. In Figure 2, multiple slice top coal caving mining is illustrated.

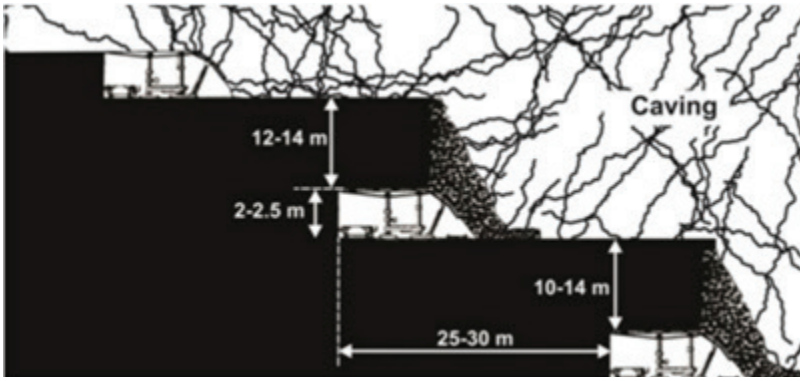

Figure 1. Multiple slice longwall with top coal caving (after Aksoy et al. 2016)

Face lengths are 180-200m and depth varies between 200 and 400m in Eynez, with discrete slicing: mining of the upper slices conventionally and after that second slice mining in the form of LTCC as described in (Başarır et al., 2015). The longwalls are being operated by the way that maximizes top coal recovery (>90%) which is achieved by allowing acceptable dilution.

Southern Soma coal mines are under projecting and development stage. At 700-1200m depth, longwall face lengths are supposed to be at least 160m and restricted by faults and other geological structures. Coal seam inclinations are below 6° with a maximum around 10°. Under great depth and extended longwall face lengths, cavability character is expected to be improved and conditions can lead to single pass LTCC production of a 16m thick coal seam which is beyond the common limits considering high recovery.

3. Cavability Assessment of Deep Coal Seam

Assessing cavability character of top coal can be dealt with several approaches namely numerical analysis and empirical methods which are mentioned in (Vakili and Hebblewhite, 2010; Aksoy et al., 2004). Still, there are limited study on the issue. In case of insufficient caving, prefracturing of top coal by blasting can be necessary. Longwall face length, support density, face advance rate, shield alignment, top coal drawing duration-sequence, set pressures of shields and other operational parameters have great impact on top coal caving success. Dattatreyulu et. al. (2012) noted that CSIRO and Chinese y-index cavability studies are based on Chinese mining cases. It should be noted that sample size in several empirical approaches are limited at the time when they were postulated and does not cover great depths.

Another cavability index work proposed by Vakili and Hebblewhite (2010), is based on numerical modelling findings which were carried out by Discrete Element Method codes. The parameters affecting cavability were found to be: deformation modulus, in-situ stress at all axes, seam thickness, spacing of vertical and horizontal jointing. Numerical modelling work was verified by several actual mining cases.

Commercially available Distinct Element Codes namely Itasca PFC, UDEC and 3DEC codes which are capable of handling discontinuum analysis was preferred (Wang et al., 2015; Hai et al., 2015) for top coal caving simulation or problems in top coal caving mines. The codes require input parameters namely discontinuity spacing, orientation, rock block geometry, discontinu-

ity deformability and discontinuity strength in addition to intact rock parameters. Continuum approaches like finite element method, finite difference method are also preferred (Yaşıtlı and Ünver, 2005; Başarır et al., 2015; Alehossein and Poulsen, 2010; Aksoy et al., 2015,2016; Xie et al., 1999) in analyzing the problems successfully, involving top coal caving.

Abutment pressure acting on the face plays an important role in fracturing of the top coal (Alehossein and Poulsen, 2010; Aksoy et al., 2015). Intact coal and roof failure and material fracturing is another essential issue in addition to structurally controlled failures. Treating the rock mass as a continuum and representing the rock mass with simple and basic rock parameters, removed the necessity of detailed input data requirements for rigorous methods. In that study utilization of numerical modelling aims to observe rock material failure in the process and investigation of top coal cavability character by utilizing and comparing convergence-confinement curves for longwall face and failure extents.

3.1. Empirical Approach

For Southern Soma deep coal mines, borehole data is taken into account and due to the absence of in-situ stress measurements, field stress was imposed according to gravitational loading and assuming horizontal to vertical stress ratio equals to unity for deep production levels. Input parameters for the approach are vertical (σv) and horizontal (σh) virgin stress, top coal thickness, modulus of Elasticity of coal (Ei), vertical (Jv) and horizontal (Jh) joint spacing values. Two outputs of Cavability index proposed by Vakili and Hebblewhite (2010) are presented below. Main caving distance (MCD) is the distance of face at a point where all top coal caves to the mined void from initial position. In cavability index, caving of the roof is not taken into account and data input is not required for roof. Top coal recovery (TCR) is the percentage of top coal recovered.

Two different depths are considered in Vakili and Hebblewhite's cavability index. Jointing, deformability values are chosen considering weak and strong sections of the coal seam. Top coal thickness of 13m is taken constant for all analyses in order to be consistent. When stronger coal seam is considered, top coal recovery is around 60% for all depths. Main caving distance (MCD) of top coal lies between 15-25m. Stronger coal seam samples fall into Class III and IV which are fair and poor cavability conditions. Weaker coal samples for all depths are expected to perform good cavability character indicated by Class II and III, good and fair cavability conditions respectively. Current practice of Soma mines include pre-fracturing blasting, slow advance rates of longwall. These practices enable production of stronger sections of top coal. According to the Table 3, even at 800m depth, it is understood that additional measures can still be necessary. This finding is examined again in further sections.

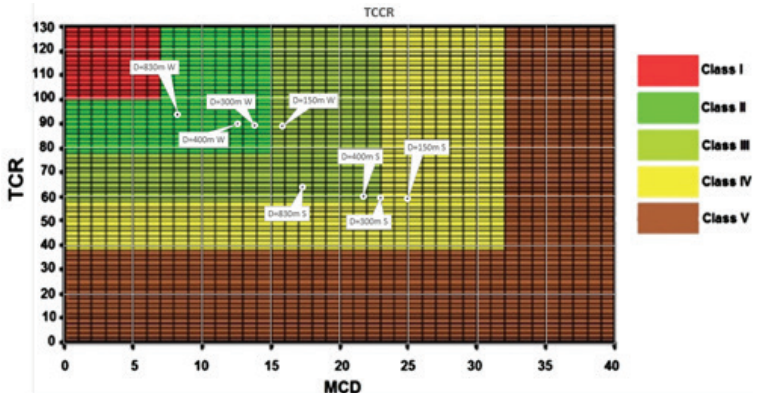

Figure 2. Top coal caving ratings on Vakili and Hebblewhite's (2010) chart

4. Numerical Modelling

Rocscience Phase^2 v.8 plane strain finite element analysis program was used in numerical modelling work in this study, (Rocscience, 2012). The plane strain program was utilized by constructing 2 axes of a longwall panel. The cross-section parallel to the face was used for examination of required longwall face length ensuring successful top coal caving and main roof. Observing tensile yielded element extent at the roof in vertical axis, displacement magnitudes reflect important data on cavability performance. Understanding the relation between numerical modelling and real mine case is essential.

Convergence-confinement curves were utilized in order to compare the top coal caving character which is a beneficial tool when a plane-strain model is in use. Convergence-confinement method is generally used in tunneling analyses (Brown et al., 1983) however, there are several researchers who used the method in longwall rock-support interaction analyses, (Barczak, 2006; Medhurst and Reed, 2005). Second cross-section generated based on the axis parallel to the longwall retreat direction was used in models. That cross-section represents the plane-strain condition in the middle of the face when a sufficiently long longwall face is established and rib side effect is diminished. Finite element mesh model is given in Figure 5.

400m and 800m deep coal seam were modelled based on same geological thicknesses, only overburden material thickness was altered. In Fig. 5, advance steps of a longwall face are visible and totally 85m face advance or retreat were simulated with 5m advance stages assuming a cutting height of 3m. In modelling work, main and tail gates were excluded and only the longwall faces were modelled. Finite element mesh density was increased gradually around the longwall faces, at the area of interest.

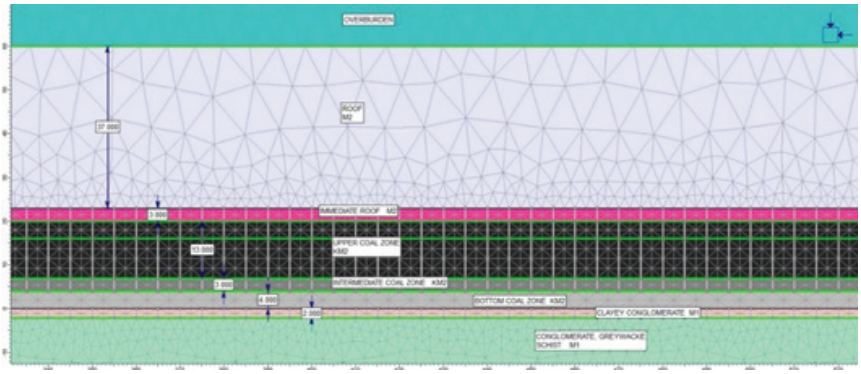

Figure 3. Zoomed view of coal seam numerical model with strata thicknesses and mesh for southern Soma coal mines

4.1. Vertical Stress Distribution, Displacements and Ground Response Interpretation

Vertical stress distribution, abutment stress and stress at face are investigated by utilizing the cross-section parallel to the longwall advance. 400m and 800m deep mining scenarios are modelled with same coal seam and main roof properties the only variable is overburden material which overlies M2 marl unit. Goaf behavior was not covered in this study and a soft goaf material was not imposed to the model. Since the model size is not sufficiently large, goaf material compaction and stress development in goaf are not possible.

Two numerical models were run with cross-sections parallel to the longwall advance: 1. Face coal cutting and removing the elements from the model without top coal drawing. 2. Removing the shearer cut zone and drawing the top coal.

In 400m deep mining case abutment stress is developed at 20m far from the face and around 15 MPa. In 800m case, abutment stress is 40-50m far from the face and between 30-35MPa. Abutment stresses are considerably far from the face which can seem unexpected since generally it is accepted that abutment stress is quite close to the face, (Figure 6). At low vertical in-situ stress and relatively strong coal presence and if elastic material behavior is assumed in order to solve similar problems which will in turn lead to high stressed, sharp vertical stress curves with peak abutment stress is close to the face.

Figure 6 shows stress distribution following a similar path when it is close to the face, since the coal seam mechanical properties and geometry are similar and the variable is depth. The face line falls on to the distance of 90m in the Figure 6. In order to have physical meaning it is better to take relative displacement from face (shield tip) to caving shield (back canopy) which is accepted as 5m for this case. In fact, the distance can be larger due to a new cut by shearer or position of back canopy flippers or equipment model. Relative displacements for conventional models are around 35 to 50 cm for 400 and 800m depth, respectively. If the model is constructed and top coal elements removed (as top coal drawing), relative displacement amounts drop around 10-20cm due to increasing horizontal displacement.

When a coal roof is established at roof in a thick coal seam, conditions considerably change when it is compared to conventional longwall operation. Generally, coal is more compressible and friable than a moderately strong roof. Top coal drawing generates a greater mined void causing difficulties in filling the goaf and compaction of the material. The advantage is, coal drawing absorb energy and cause loosening of the upper zones. If the advance rate of the longwall face can be adjusted, LTCC shields can be more satisfactory operated by means of ensuring support capacity.

Ground response behavior was investigated by considering 3 different longwall face lengths (60, 160,200m) at two different depths (400 and 800m). Plane strain models were constructed based on the cross-section parallel to face. Internal stress reduction was applied on to the boundary of the longwall face. Internal stress reduction was applied in 10 stages.

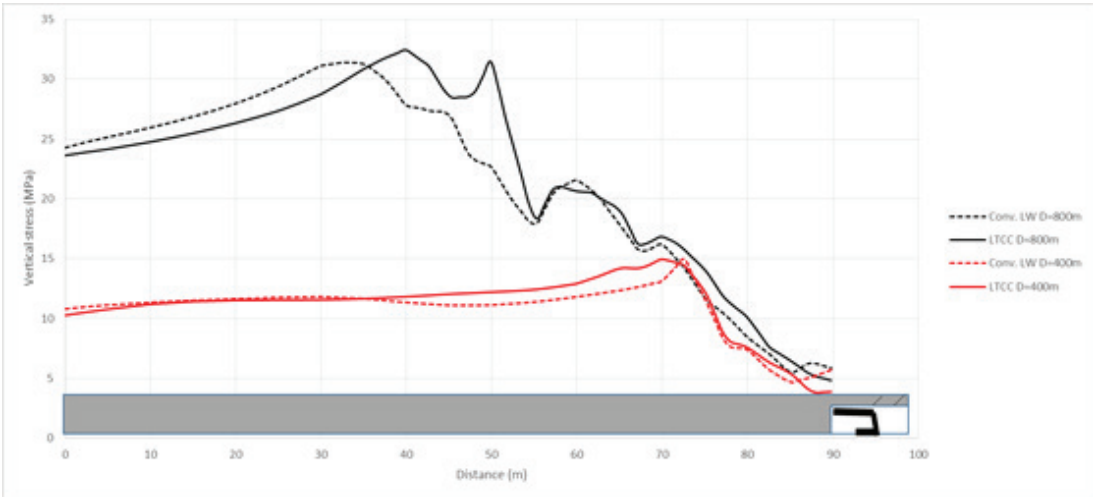

Figure 4. Vertical stress distribution along the mid-face for different depth and mining methods

Ground response curves are plotted for seams having depth of 400 and 800m. Additionally, longwall face lengths of 60, 160 and 200m. Support densities for longwall face supports are

generally around 1 MPa or lower. Those support pressures cannot be compared to stress carried by face itself. For the case in this study, vertical stress at face are found to be around 4 to 6 MPa. Then, it is obviously the major supporting element is face itself. Longwall support carries dead rock load, improves bedding interlocking and reducing bedding separation then it ensures stability for the face environment. However, if the roof will converge, it is not totally resistible by typical shield support pressures and then it will finally converge.

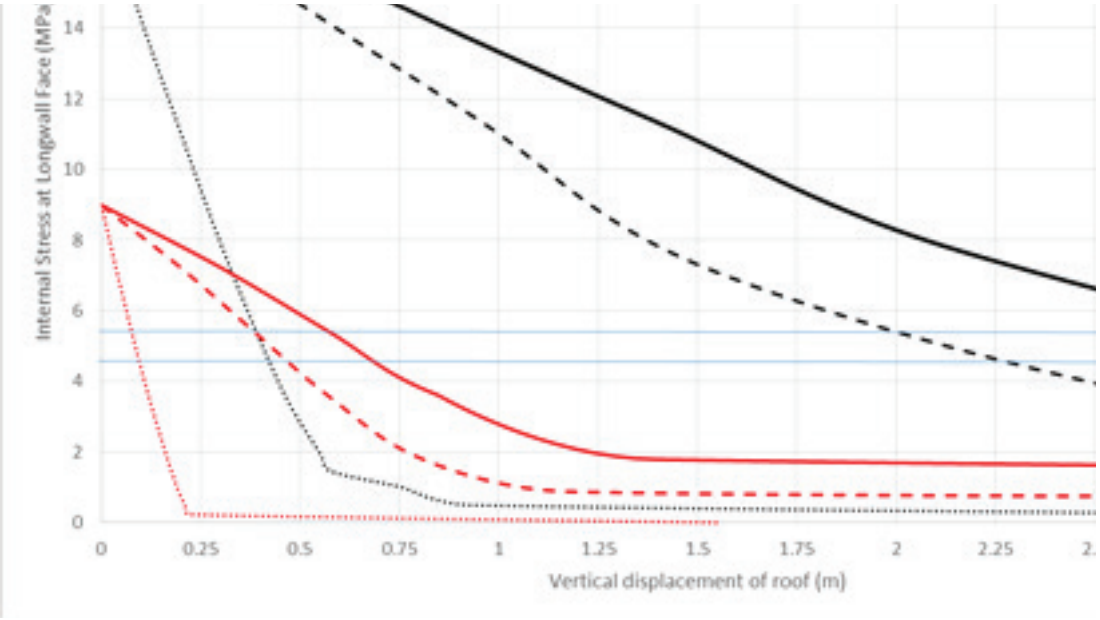

Figure 5. Ground response behavior for 400 and 800m depths and different face lengths

Vertical stress range at face for two different depths are labelled in Figure Below and represents the point on ground reaction curve at face. Previously mentioned empirical approaches does not consider face lengths. When we examine the problem by comparing face lengths, 60m long faces obviously seem to have less deformation potential. For same internal stress reduction on longwall face boundary, deformation attained is considerably small. Same conclusion can be suggested by considering the slopes of the curves in 4-6MPa range. In Soma coal basin, there are many longwalls under operation with 60-80m long faces. Caving of the roof as well as top coal caving are commonly faced problems especially for the first panel of a sector. Current mining activity mostly suggests caving of the roof first by operating a conventional longwall along the upper most slice of the seam. When mine induced deformation and stress have great impact on a particular area, then even in longwalls with short face, roof or top coal caves more easily. Ground reaction curves suggest for 16m thick coal seam, a single pass LTCC operation will not have sufficient top coal caving for both depth cases.
160 to 200m long longwall faces are expected to have similar caving tendency. Other finding is shields may yield up to 35 to 50 cm for 400 and 800m depth, respectively. Of course caving and convergence is strongly related to face advance pace.

5. Conclusions

Ground reaction curves provide valuable data on the relation between face length and cavability character of top coal where empirical approaches do not consider. Same methodology in the study can also be applied in order to foresee roof caving behavior for a conventional longwall. It is obvious that accurate findings can be obtained by construction of a pre-existing longwall and

calibrated data can be imposed to new problem. The methodology is also beneficial in case of utilizing numerical modelling programs assuming plane-strain even though three-dimensional approaches will probably give better estimates in turn more effort and time will be required.
In addition to the scientific facts operational factors have great impact on top coal caving and roof control success. Proper alignment of the longwall shields, optimized caving sequence and interval, clock work of the equipment, absence or presence of malfunctioning or leaking supports and more items are important and have direct effect on the success of a LTCC operation. Another critical parameter is longwall advance rate: slow advance increases degradation of the rock mass increases loads on the supports while it improves caving of top coal. Additionally, during a longwall advance ground stress distribution will change but not immediately. Occasions where peak abutment stress may stay closer to the face when longwall face advance is relatively fast, yielded zone at face may be reduced. In order to simulate that behavior, imposing time dependent properties with extensive calibration effort is necessary.

References

Aksoy, C.O., Kose, H., Onargan, T., Koca, Y., Heasley, K., 2004. Estimation of limit angle using laminated displacement discontinuity analysis in the Soma coal field, Western Turkey. International Journal of Rock Mechanics & Mining Sciences, 547–556.

Aksoy, C.O., 2005. Three-dimensional finite element analysis of an undermined shaft at the Hustas mine, Turkey. CIM Bulletin vol. 98, N° 1089 Paper 38

Aksoy, C.O., Küçük ,K., Uyar, G.G., 2015. Safety Pillar Design for Main Galleries in Multi-Slice Longwall Top Coal Caving Method, International Journal of Oil Gas and Coal Technology, 9(3), 329-347.

Aksoy, C.O., Küçük, K., Uyar, G. G., 2016. Long-term time-dependent consolidation analysis by numerical modelling to determine subsidence effect area induced by longwall top coal caving method. International Journal of Oil Gas and Coal Technology, 12(1), 18-37.

Alehossein, H., Poulsen, B.A., 2010. Stress analysis of longwall top coal caving. International Journal of Rock Mechanics and Mining Sciences, 47, 30–41.

Barczak, T.M., 2006. A retrospective assessment of longwall roof support with a focus on challenging accepted roof support concepts and design premises. Proceedings, 25th International Conference on Ground Control in Mining, Morgantown, WV, 232-244.

Basarir, H., Öge, İ.F., Aydin, O., 2015. Prediction of the stresses around main and tail gates during top coal caving by 3D numerical analysis. International Journal of Rock Mechanics and Mining Sciences, 76, 88-97.

Brown, E.T., Bray, J.W., Ladanyi, B., Hoek, E., 1983. Ground Response curves for rock tunnels. Journal of Geotechnical Engineering, 109, 15-39

Cai, M,. Kaisera, P.K., Tasaka, Y., Minami, M., 2007. Determination of residual strength parameters of jointed rock masses using the GSI system. International Journal of Rock Mechanics & Mining Sciences, 44, 247–265

Dattatreyulu, J.V., Khanal, M., Adhikary, D., Balusu, R., 2012. Geotechnical studies for introducing high capacity longwalls and longwall top coal caving mining in SCCL: a case study. Proceedings of the 4th Coal Summit, New Delhi, India.

Doktan, M., İnci, Y., 1986. The Production Method Adapted in Underground Pits of ELl-Soma Region and Possibilities of Mechanisation. Madencilik, 25, 5-20 (in Turkish)

Doktan, M., İnci, Y., 1987. Status of thick seam coal mining over the world and in Turkey. 10th Turkey Scientific and Technical Congress, Ankara, 51-65. (in Turkish with English abstract).

Hai, S., Jianbiao, B., Shuai, Y., Yong, C., Zizheng, Z., 2015. Study on gob-side entry retaining in fully-mechanized longwall with top-coal caving and its application. International Journal of Mining Science and Technology, 25, 503–510

Hoek, E., Carranza-Torres C., Corkum B., 2002. Hoek-Brown failure criterion – 2002 Edition. Proceedings NARMS-TAC Conference, Toronto, 267-273.

Hoek, E., Carter, T.G., Diederichs, M.S., 2013. Quantification of the Geological Strength Index chart. Proceedings 47th U.S. Rock Mechanics/Geomechanics Symposium, California, 2013. ARMA 13-672,1-8.

Huang, B., Wang, Y., Cao, Y., 2015. Cavability control by hydraulic fracturing for top coal caving in hard thick coal seams. International Journal of Rock Mechanics & Mining Sciences, 74, 45–57.

Humphries, P., Poulsen, B., 2008. Geological and Geotechnical Influences on the Caveability and Drawability of Top Coal in Longwalls. Aziz N (ed), Coal 2008: Coal Operators' Conference, University of Wollongong & the Australasian Institute of Mining and Metallurgy, 56-66.

Marinos, V., 2014. Tunnel behaviour and support associated with the weak rock masses of flysch. Journal of Rock Mechanics and Geotechnical Engineering, 6, 227-239

Medhurst, T.P., Reed, K., 2005. Ground response curves for longwall support assessment. Transactions of the Institution of Mining and Metallurgy, 114, A81-88.

Rocscience, Inc., 2012. Phase2, V.8. Rocscience Inc., Toronto, Canada

Vakili, A., Hebblewhite, B.K., 2010. A new cavability assessment criterion for Longwall Top Coal Caving. International Journal of Rock Mechanics and Mining Sciences, 47, 1317–1329.

Wang, J., Zhang, J., Song, Z., Li, Z., 2015. Three-dimensional experimental study of loose top-coal drawing law for longwall top-coal caving mining technology. Journal of Rock Mechanics and Geotechnical Engineering, 7, 318-326

Xie, H., Chen, Z., Wang, J., 1999. Three-dimensional numerical analysis of deformation and failure during top coal caving, International Journal of Rock Mechanics & Mining Sciences, 36, 651-658

Yasitli, NE, Unver, B.,2005. 3D Numerical modeling of longwall mining with top-coal caving. International Journal of Rock Mechanics and Mining Sciences, 42, 219–35.

Yılmaz, A. I., Büyükyıldız, G., Ekici, A., Çalık, M., Önder, Ö., Aksoy, C.O., 2013. Staff transportation two way on the belt conveyor, Acta Montanistica Slovaca, 18(3), 141-150.

Makale Gönderim Tarihi:27.07.2016
Yayına Kabul Tarihi:17.08.2016

Reliability Analysis of Loader Equipment: A Case Study of a Galcheshmeh Travertine Quarry in Iran

Mehdi Taherı [1], Abbas Aghajani Bazzazı[2]*
[1] *Department of Mining Engineering, Islamic Azad University, Tehran, Iran*
[2] *Department of Mining Engineering, University of Kashan, Kashan, Iran*
**Corresponding Author: a_aghajani_bazzazi@kashanu.ac.ir*

Abstract
Unplanned equipment failures and their consequences have significant influence on the total operating cost of a mining system. Loader is one of the main machinery in quarry mines. From an economic point of view, more than 50 % of production costs in quarry mines are allocated to hauling and loading costs, so it is important to keep equipment in good condition. Reliability is a useful tool for evaluating the performance of this machine. In this research, the reliability analysis of loading equipment in Galcheshmeh travertine quarrying which consists of two loaders has been analyzed. In this study, two approaches were considered for analyze maintenance data, namely a basic maintenance approach and a reliability based approach. Trend and serial correlation test were applied to validate the assumption of independent and identically distribution (IID). For finding the best-fit distribution, different types of statistical distributions were tested by the Easyfit software. The developed model based on these data showed that the reliability of the loader No. 1 and Bo. 2 decreases to a zero value after approximately 477 hours and 309 hours of operation, respectively. To achieving the high reliability a review on maintenance program must be performed.

Keywords: Reliability analysis, Maintenance, Failure, Probability distribution, Galcheshmeh travertine quarry.

1. Introduction

Technological development has enabled the mining industry to deploy more complex and capital-intensive equipment to increase productivity, but inefficient operation and deficient maintenance often prevent utilization of its full capacity. Interest in the maintenance and operational reliability of all capital-intensive equipment has been stimulated by the current emphasis on reducing production costs. Reliability analysis techniques have been gradually accepted as standard tools for the planning and operation of automatic and complex mining systems since the mid-1980s (Kumar et al., 1989). The most important reliability studies were presented in Table 1.

2. Basic Concept and Approach for Reliability Analysis

1. Mean Time To Repair (MTTR): The mean time required to repair a component, expressed as the total repair time divided by the total number of repairs.
2. Percentage of Total Repairs: The percentage of total repairs, expressed as the repair frequency of a system divided by total repair frequency for all systems.
3. Mean Time Between Failures (MTBF): The mean time of the failure distribution of a machine or component. For a constant failure rate it is expressed as the total operating time divided by the total number of repairs.
4. Availability: The percentage of time that a system is operating satisfactorily. It is represented by the following equation.

$$Availibity = \frac{MTBF}{MTBF + MTTR} \tag{1}$$

5. Reliability: The probability that a system or component will operate without failure under a given condition for a specified time period (Esmaeili et al., 2011).

$$R(t) = 1 - F(t) \tag{2}$$

Table 1. Summary of the literature review

Date	Author	Title	Software used
1989	Kumar et al.	Reliability Investigation for a Fleet of Load Haul Dump Machines in a Swedish Mine	STATGRAPHICS
1994	Vagenas et al.	Analysis of truck maintenance characteristics in a Swedish open pit mine	-
2000	Nuziale & Vagenas	A software architecture for reliability analysis of mining equipment	RelSoft & Architecture
2001	Roy et al.	Maintainability and reliability of a fleet of shovels	-
2008	Barabady & Kumar	Reliability analysis of mining equipment: A case study of a crushing plant at Jajarm Bauxite Mine in Iran	Weibull++6
2011	Esmaeili et al.	Reliability analysis of a fleet of loaders in SANGAN iron mine	Easy Fit
2014	Furuly et al.	Availability analysis of the main conveyor in the Svea Coal Mine in Norway	Weibull++7

3. Case Study

Here we present a case study describing the reliability analysis of two Caterpillar loaders (988B No.1 and 988B No.2). These data collected over a time period of 9 months (from April 2015 to

December 2015) for loader No.1 and a time period of 6 months (from June 2015 to November 2015) for loader No.2 by using hand written forms prepared by maintenance personal, daily report and maintenance cards. These maintenance cards include time to failure, the machine hour meter and the time to repairs.

Before analyzing the machine's characteristics and failure data, the machine should be classified into a number of systems and subsystems in order to categorize the types of failure occurring on the machine. These classifications will depend on the maintenance records kept by maintenance personnel, as well as the reasoning describing these records (Vagenas et al., 2003).

In this paper preventive maintenance is applied as a subsystem in order to ensure a proper maintenance. Preventive maintenance defined as the actions performed in attempt to retain an item in a specified condition by providing systematic inspection, detection and prevention of incipient failure (Oyebisi 2000; Paraszczak and Perreault, 1994). Useful classification subsystem for a fleet of two loaders was presented in Table 2.

Table 2. Useful classification subsystem for loaders

	Subsystem	Code
Loader No.1	1. Transmission	TRAN
	2. Hydraulic	HYD
	3. Others (Engine, Electrical, Structural, Bucket, Braking)	OTH
Loader No.2	1. Tire	TR
	2. Others (Engine, Structural, Bucket)	OTH

3.1. Data Collection, Sorting and Classification

Three basic steps have been performed before data analyzing for determining reliability Characteristics. These are data collection from different sources of data in mine equipment, sorting of the data required for analysis and data classification in the form required for the analysis (time between failures (TBF), time to repair (TTR), repair frequency, total breakdown hours, total working hours, total maintenance hours, etc.) (Barabady and Kumar, 2008).

We design our own tables in order to sort and arrange the data in a chronological order. The part of the data collected for loader No.1 and No.2 are given in Table 3 and 4, respectively.

Table 3. A part of failure data for reliability based analysis of loader No. 1

No.	Systems repaired	TTR (hours)	Cumulative TTR	TBF (hours)	Cumulative TBF
1	OTH(Electrical)	3	3	5	5
2	HYD	1	4	1	6
3	HYD	1	5	2	8
4	TRAN	2	7	5	13
5	TRAN	3	10	80	93
6	TRAN	6	16	20	113
7	TRAN	26	42	70	183
8	TRAN	40	82	140	323

9	TRAN	23	105	70	393
10	TRAN	24	129	60	453
11	TRAN	28	157	70	523
12	HYD	1	158	10	533
13	OTH(Braking)	5	163	9	542
14	OTH(Bucket)	20	183	50	592
15	HYD	1	184	2	594
16	HYD	1	185	12	606
17	HYD	5	190	6	612
18	OTH(Structural)	5	195	10	622
19	OTH(Engine)	10	205	60	682
20	OTH(Electrical)	6	211	30	712

Table 4. A part of failure data for reliability based analysis of loader No. 2

No.	Systems repaired	TTR (hours)	Cumulative TTR	TBF (hours)	Cumulative TBF
1	OTH(Engine)	3	3	30	30
2	OTH(Bucket)	19	22	20	50
3	OTH(Structural)	3	25	10	60
4	TR	18	43	60	120
5	TR	3	46	10	130
6	OTH(Structural)	19	65	50	180
7	OTH(Bucket)	31	96	80	260
8	TR	2.5	98.5	50	310
9	TR	3.5	102	60	370
10	TR	4	106	80	450

3.2. Analysis Using Graphical Methods

The next step was analyzed data by graphical methods in order to evaluate parameter such as repair frequency, time between failures (TBF), time to repair (TTR), total working hours and total repair time. The TBFs and TTRs for subsystems are calculated. Repair frequency, total repair time, percent of total repairs, minimum and maximum for each type of failure for two loaders provides in Table 5. The data from Table 5 may be better visualized in figures 1 and 2 for loader No. 1 and figures 3 and 4 for loader No. 2. Figure 1 displays the percent of total repairs and repair frequency versus type of failure. By studying Figure 2, it can be seen that the transmission and hydraulic are the most frequently occurring repairs for loader No. 1 and consume the most repair time. Also by studying Figure 3, it can be seen that the tire is the most frequently occurring repairs to loader No. 2 and consume the most repair time. Figures 2 and 4 have been provided a plot of repair frequency and repair time versus type of failure. These graphs provide a better view of failure trends of equipment. A summary of the operating time, total number of repairs, and total repair hours for two loaders provides in Table 6. In this table, availability is calculated by Equation 1.

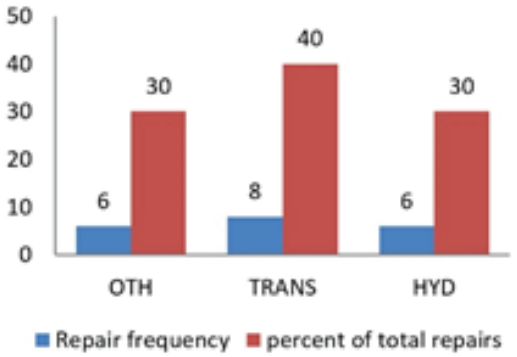

Figure 1. Repair frequency and percent of total repairs versus type of failure for loader No. 1

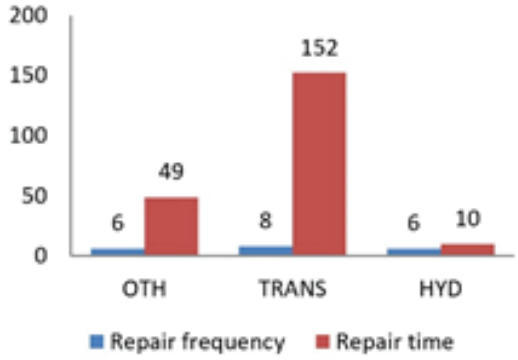

Figure 2. Repair time and repair frequency versus type of failure for loader No. 1

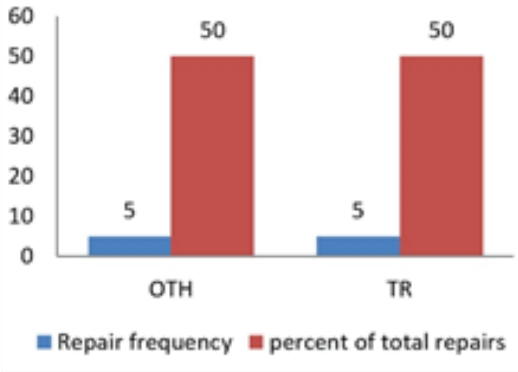

Figure 3. Repair frequency and percent of total repairs versus type of failure for loader No. 2

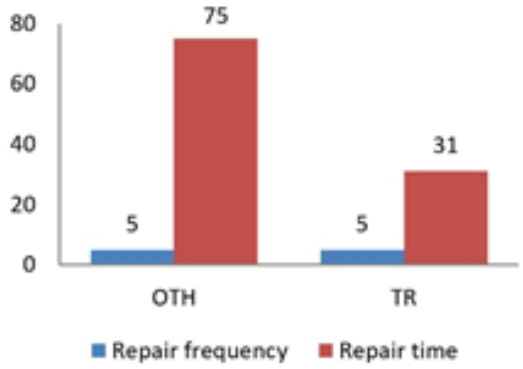

Figure 4. Repair time and repair frequency versus type of failure for loader No. 2

Table 5. An overall view of the maintenance characteristics for each type of failure

Loader No. 1	Type of Failure	TRAN	HYD	OTH	Loader No. 2	TR	OTH
	Repair frequency	8	6	6		5	5
	Repair time	152	10	49		31	75
	Percent of total repairs	40	30	30		50	50
	Min	2	1	3		2.5	3
	Max	40	5	30		18	31
	Avg	19	1.7	8.2		6.2	15

Table 6. The summary of failure characteristics of a fleet of two loaders

	Loader No. 1	Loader No. 2
Operating Hours	447	309
Total Number of Repairs	20	10
Total Repair Hours	211	106
MTTR (Hours)	10.55	10.6
MTBF (Hours)	23.9	30.9
Availability	69.3%	74.5%
Fleet Availability (Average of availability of two loaders)	71.89%	

3.3. Trend Test and Serial Correlation

The next step after the collection, sorting and classification of data is the validation of the Independent and Identically Distributed (IID) nature of the TBF and TTR data of each subsystem. The computed values of the test statistic for the different subsystem failures and repairs' data are given in Table 3 and 4. A trend test involves plotting the cumulative failure number against the cumulative time between failures. Fig. 5 illustrates the trend test for loader No. 1 and No. 2. As can be seen in Fig. 5 trend test shows a straight line and it means that the data is free of trend.

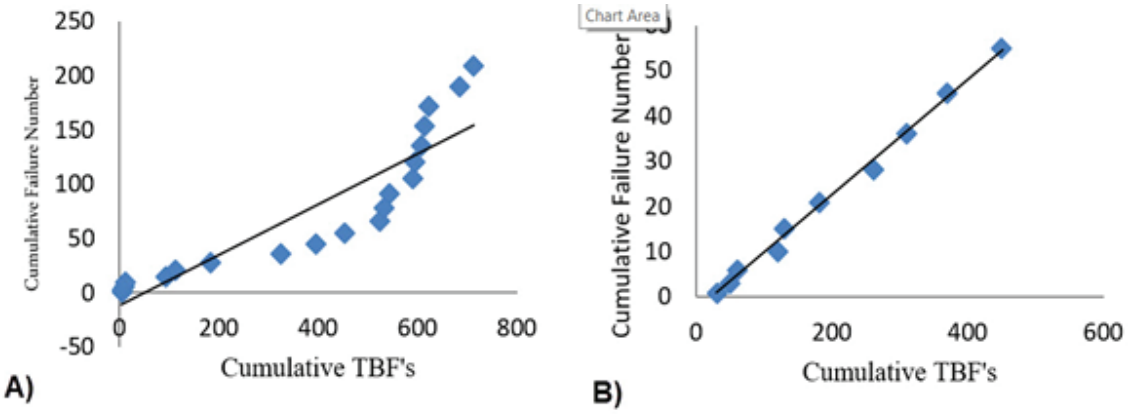

Figure 5. A) Trend plot for loader No. 1 and B) trend plot for loader No. 2

The serial correlation test is a plot of the data pairs (Xi, Xi–l) for i = 1, …, n, where n is the failure number. A scatter plots of the time between failures (TBF) for loader No. 1 and No.2 are displayed in Figure 6. They show that the points are scattered randomly throughout the plots. This indicates that the data is free of the correlations and can be assumed to be independent.

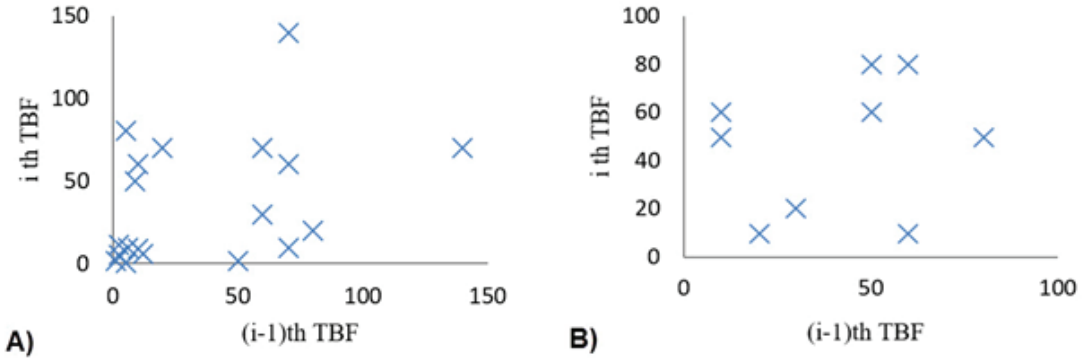

Figure 6. A) Scatter plot for test serial correlation for loader No. 1 and B) Scatter plot for test serial correlation for loader No. 2

Thus the assumption of independent and identically distributed (IID) data for all two loaders should be accepted and consequently the data can be fitted to theoretical probability distributions for reliability calculations.

3.4. Reliability Estimation

The next step is to assess the goodness-of-fit of a probability distribution model to the failures. One of the most widely used non parametric test for assessing the goodness-of-fit of repair times and time between failures is the Kolmogorov-Smirnov (K-S) test (Paraszczak and Perreault, 1994; Kumar and Vagenas, 1993). The K-S test examines for differences between the theoretical distribution and the observed cumulative distribution. This test can easily be performed by a probability distribution fitting software package. The data for the two loaders were tested for goodness-of-fit. Five distribution methods such as Weibull 2 parameter, Weibull 3 parameter, Exponential 1parameter, Exponential 2 parameter and Lognormal were fitted to the time between failures (TBF) data. Table 7 and 8 illustrates the results of these tests for the TBF data using the Easy-Fit software. This software assesses the goodness-of-fit of a probability distribution to the data by theoretical probability distributions.

Table 7. Goodness of fit for determination of best fit distribution for the TBF data of loader No. 1

K-S test (goodness-of-fit)						Best fit	Parameters
Sub-system	Weibull2 parameter	Log normal	Exponential 2 parameter	Weibull3 parameter	Exponential 1 parameter		
TRAN	0.3283	0.3495	0.3539	0.3865	0.3562	Weibull2 parameter	$\alpha = 0.81718$
							$\beta = 71.788$
HYD	0.2083	0.2549	0.3007	0.3231	0.1951	Exponential 1parameter	$\lambda = 0.18182$
OTH	0.2141	0.2458	0.2994	0.2549	0.1936	Exponential 1parameter	$\lambda = 0.03659$
Machine	0.1736	0.1818	0.2276	0.1642	0.2138	Weibull3 parameter	$\alpha = 0.61645$
							$\beta = 26.969$
							$\gamma = 1.0$

The next step after determination of the best fit distribution is reliability estimation of the entire machine and their subsystems using the reliability function of the fitted distribution (Equation 2). The required functions provided in Table 9 and then the reliability of the two loaders was calculated (Table 10). Figures 7 and 8 display the results of the reliability estimation for the operation hours of each subsystem of loader No. 1 and No. 2, respectively.

Table 8. Goodness of fit for determination of best fit distribution for the TBF data of loader No. 2

K-S test (goodness-of-fit)						Best fit	Parameters
Sub-system	Weibull2 parameter	Log normal	Exponential 2 parameter	Weibull3 parameter	Exponential 1 parameter		
TR	0.3658	0.3993	0.4321	0.4773	0.4321	Weibull2 parameter	α = 0.85043
							β = 61.87
OTH	0.2095	0.1619	0.2	0.1771	0.2313	Lognor-mal	σ =0.72032
							μ = 3.3987
Machine	0.2394	0.2713	0.2811	0.3452	0.2708	Weibull2 parameter	α = 1.2046
							β = 49.178

Table 9. Required functions for reliability analysis

Distribution	Density function	Distribution function
Weibull2 Parameter	$f(x)=\frac{\alpha}{\beta}(\frac{x}{\beta})^{\alpha-1}\exp(-(\frac{x}{\beta}))^{\alpha}$	$F(x)=1-\exp(-(\frac{x}{\beta}))^{\alpha}$
Weibull3 Parameter	$f(x)=\frac{\alpha}{\beta}(\frac{x-\gamma}{\beta})^{\alpha-1}\exp(-(\frac{x-\gamma}{\beta}))^{\alpha}$	$F(x)=1-\exp(-(\frac{x-\gamma}{\beta}))^{\alpha}$
Exponential 2 parameter	$f(x)=\lambda\exp(-\lambda(x-y))$	$F(x)=1-\exp(-\lambda(x-y))$
Lognormal 2 parameter	$f(x)=\frac{\exp(-\frac{1}{2}(\frac{\ln(x)-\mu}{\sigma})^2)}{x\sigma\sqrt{2\pi}}$	$F(x)=\Phi(\frac{\ln(x)-\mu}{\sigma})$
Exponential 1 parameter	$f(x)=\lambda\exp(-\lambda x)$	$F(x)=1-\exp(-\lambda x)$

Table 10. Reliability estimation for two loaders

Loaders	Best fit	Parameter	Reliability estimation	Operation hours
Loader No. 1	Weibull3 parameter	α = 0.61645	2.8 × 10-3	477
		β = 26.969		
		γ = 1.0		
Loader No. 2	Weibull2 parameter	α = 1.2046	1.06 × 10-4	309
		β = 49.178		

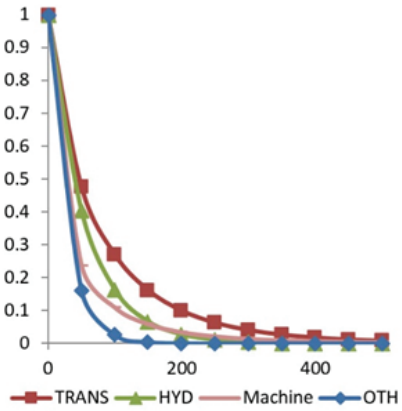

Figure 7. A plot for reliability estimation of loader No. 1

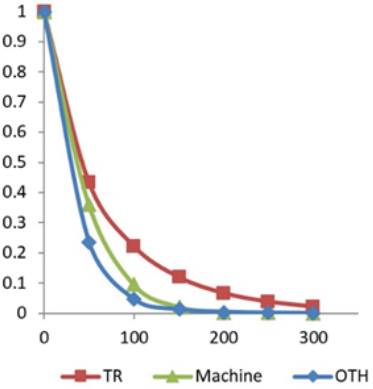

Figure 8. A plot for reliability estimation of loader No. 2

4. Conclusions

Reliability and maintainability of mining industry is more in focus than ever, and the mining systems are becoming more complex and the equipment more expensive to repair or modify. In this paper, the case study shows that the transmission and hydraulic in the loader No. 1, the tire in the loader No. 2, are the most frequency occurring repairs and consume the most repair times. These subsystems are critical from a reliability point of view. The Weibull distribution provided the best fit distribution, in the most cases, to the time between failures data of two loaders. Then, the loaders No. 1 and No. 2 reliability for the operation hours have been predicted, 2.8×10-3, 1.06×10-4 respectively. The reason of the low reliability of loaders can be expressed closed to end of working life. This study shows that the reliability analysis is very useful for deciding maintenance intervals.

References

Barabady, J., Kumar, U., 2008. Reliability analysis of mining equipment: A case study of a crushing plant at Jajarm Bauxite Mine in Iran. Reliability Engineering and System Safety, 93, 647-653.

Esmaeili, M., Aghajani, A., 2011. Reliability analysis of a fleet of loaders in Sangan Iron Mine. Archives of mining sciences, 56, 629-640.

Furuly, S., 2014. Availability analysis of the main conveyor in the Svea Coal Mine in Norway. International Journal of Mining Science and Technology, 24, 587–591.

Kumar, D., Vagenas, N., 1993. Performance evaluation of an automatic load-haul dump vehicle. CIM Bulletin, 86, 39-42.

Kumar, U., Klefsjö, B., Granholm, S., 1989. Reliability Investigation for a Fleet of Load Haul Dump Machines in a Swedish Mine. Reliability Engineering and System Safety, 26, 341-361.

Nuziale, T., Vagenas, N., 2000. A software architecture for reliability analysis of mining equipment. International Journal of Surface Mining, Reclamation and Environment, 114, 19-34.

Oyebisi, T.O., 2000. On reliability and maintenance management of electronic equipment in the tropics. Technovation, 20, 517-522.

Paraszczak, J., Perreault, J.F., 1994. Reliability of diesel powered Load-Haul-dump machines in an underground Quebec mine. CIM Bulletin, 87, 123-127.

Roy, S.K., Bhattacharyya M.M., Naikan V.N.A., 2001. Maintainability and reliability of a fleet of shovels. Mining Technology, 110, 163-171.

Vagenas, N., Kazakidis, V., Scoble, M., Espley, S., 2003. Applying a maintenance methodology for excavation reliability. International Journal of Surface Mining, Reclamation and Environment, 17, 4-19.

Vagenas, N., Kumar, U., Rönnkvist, E., 1994. Analysis of truck maintenance characteristics in a Swedish open pit mine. International Journal of Surface Mining, Reclamation and Environment, 8, 65-71.

Makale Gönderim Tarihi:23.07.2016
Yayına Kabul Tarihi:29.08.2016

Optimization of Copper Extraction from Advanced Milled Chalcopyrite Concentrate with Hydrogen Peroxide Leaching

M. Deniz Turan [1]*, Z. Abidin Sarı [1], Hasan Nizamoğlu [1], Yunus Elmas [1]
[1] Firat University, Dept. of Metallurgical and Materials Engineering, 23119, Elazig, Turkey
**Corresponding Author: mdturan@firat.edu.tr*

Abstract
Response surface methods (RSM) have some advantages such as easy optimization, to reach results quickly, and availability of evaluation statistically. Because of these reasons, the experiments were designed by using RSM. In this study, copper extraction was investigated from advanced milled chalcopyrite concentrate by using hydrogen peroxide as oxidant and acetic acid as stabilizer. In this context, effects of different parameters were studied such as grinding time, leaching time, peroxide concentration, and leaching temperature. Results showed that nearly 100% of copper was extracted compatible statistically (R^2=0.8072) while the most effective parameter was defined the changing of hydrogen peroxide concentration.

Keywords: Chalcopyrite, Optimization, Leaching, Peroxide.

1. Introduction

Among the copper sulfides used to produce metallic copper, chalcopyrite (CuFeS2) is the predominant mineral. The concentrates of chalcopyrite are generally treated by pyrometallurgical methods of smelting and converting processes to win the copper metal. However, this high temperature route has always been plagued with environmental issues concerning pollution not only with SO2 gas emissions but also with emissions of toxic compounds of arsenic, antimony, and other heavy metals. (Padilla, et al., 2007)

Hydrometallurgical processes offer great potential for treating sulphide concentrates such as chalcopyrite concentrate. On the other hand, leaching of chalcopyrite is difficult and strong oxidant or pressure conditions must be used. These effective conditions are usually provided by using oxygen gas in the autoclave system (Padilla, et al., 2008; McDonald and Muir, 2006a; McDonald and Muir, 2006b), but feeding gas into a pressure autoclave system may be difficult and costly.

The chalcopyrite leaching by hydrogen peroxide can be summarized as (Misra, et al., 2007),

$$CuFeS_2 \rightarrow Cu^{2+}+Fe^{2+}+2S^{2-} \quad (1)$$

$$S^{2-} \rightarrow 4e^{-}+2S^{o} \quad (2)$$

$$2H_2O_2+4H^{+}+4e^{-} \rightarrow 4H_2O \quad (3)$$

2. Results and Discussion

2.1. Materials and Methods

Chalcopyrite concentrates namely Ergani concentrate was obtained from Elazig, Turkey. This concentrate was classified by sieving through 200 mesh. The fraction passed (90 % of total mass) through this sieve was used in all experiments. For the chemical analyses of the chalcopyrite concentrate, sample was dissolved by using microwave-assisted acid dissolution technique. After the dissolution, chemical analyses of clear supernatant were carried out by ICP-OES (Perkin-Elmer Optima 2000 DV). Sulphur content of the concentrate was determined gravimetrically. Mineralogical analyses of the concentrate were made by using X-ray diffraction system (Shimadzu XRD-6000) and powder diffraction technique. X-ray diffraction results showed that dominant mineral phases are chalcopyrite ($CuFeS_2$) and pyrite (FeS_2).
Chalcopyrite concentrate sample containing 28.31wt%Cu, 28.52 wt%Fe, 29.36wt%S was used for experiments.

Leaching experiments were performed under atmospheric conditions by using a conventional magnetic multi stirrer (Velp Scientific MultiStirrer 15). At the end of the leaching period, the contents were cooled and filtered. Filtered solutions were analyzed for copper using an AAS (Perkin Elmer-Analyst 400).

Box-Behnken experimental design was used. The experimental variables and their corresponding levels are listed in Table 1.

Table 1. Experimental range and levels of the independent variables.

Experimental parameters	Symbol	Unit	Low Level	High Level
Milling time	A	min	1	39
Leaching time	B	min	5	115
Leaching temperature	C	°C	25	65
H_2O_2 concentration	D	M	0.1	3.9

2.2. Experimental Results

The results of the experiments for each experimental condition are shown in Table 2. As seen in Table 2, the experiments were planned as a total of 29 runs that included 5 center points. The effects of various leaching variables on metal extraction were studied. According to the results, the following variables are of significance as; grinding time, leaching time, peroxide concentration, and leaching temperature. It is clear that high copper extraction can be achieved with long milling time and high leaching temperature. Effect of leaching temperature was examined as seen in Table 2. It is evident that increasing temperature was caused to higher copper dissolution. However, it was observed that the leaching yield decrease at state high concentrations of hydrogen peroxide. Possible reason for this, hydrogen peroxide is an unstable compound, whose decomposition can be catalyzed by certain factors such as the presence of an acid, base, mineral surface or soluble ions. Due to rapid exothermic decomposition of hydrogen peroxide in solution, isothermal leaching conditions may disappear and the active oxygen may not be sufficiently used for oxidation of sulfide minerals in the leaching system. Therefore, to avoid rapid decomposition of hydrogen peroxide, acetic acid was used in the experiments. As a result, it is a group of graphs as follows shows the interaction effect of various parameters on the result (Figure 1).

Table 2. Experimental design with actual factors and observed results

Run	A	B	C	D	Cu %
1	1.00	5.00	45.00	2.00	35.5
2	39.00	5.00	45.00	2.00	68.5
3	1.00	115.00	45.00	2.00	59.8
4	39.00	115.00	45.00	2.00	91
5	20.00	60.00	25.00	0.10	10.56
6	20.00	60.00	65.00	0.10	8.5
7	20.00	60.00	25.00	3.90	21.48
8	20.00	60.00	65.00	3.90	28.58
9	1.00	60.00	45.00	0.10	5.38
10	39.00	60.00	45.00	0.10	9.60
11	1.00	60.00	45.00	3.90	80.93
12	39.00	60.00	45.00	3.90	40.57
13	20.00	5.00	25.00	2.00	54.88
14	20.00	115.00	25.00	2.00	62.25
15	20.00	5.00	65.00	2.00	67.50

Run	A	B	C	D	Cu %
16	20.00	115.00	65.00	2.00	100
17	1.00	60.00	25.00	2.00	40.86
18	39.00	60.00	25.00	2.00	68.43
19	1.00	60.00	65.00	2.00	56.25
20	39.00	60.00	65.00	2.00	91.7
21	20.00	5.00	45.00	0.10	9.65
22	20.00	115.00	45.00	0.10	10.40
23	20.00	5.00	45.00	3.90	62.76
24	20.00	115.00	45.00	3.90	32.65
25	20.00	60.00	45.00	2.00	64.59
26	20.00	60.00	45.00	2.00	67.33
27	20.00	60.00	45.00	2.00	65.76
28	20.00	60.00	45.00	2.00	61.30
29	20.00	60.00	45.00	2.00	61.83

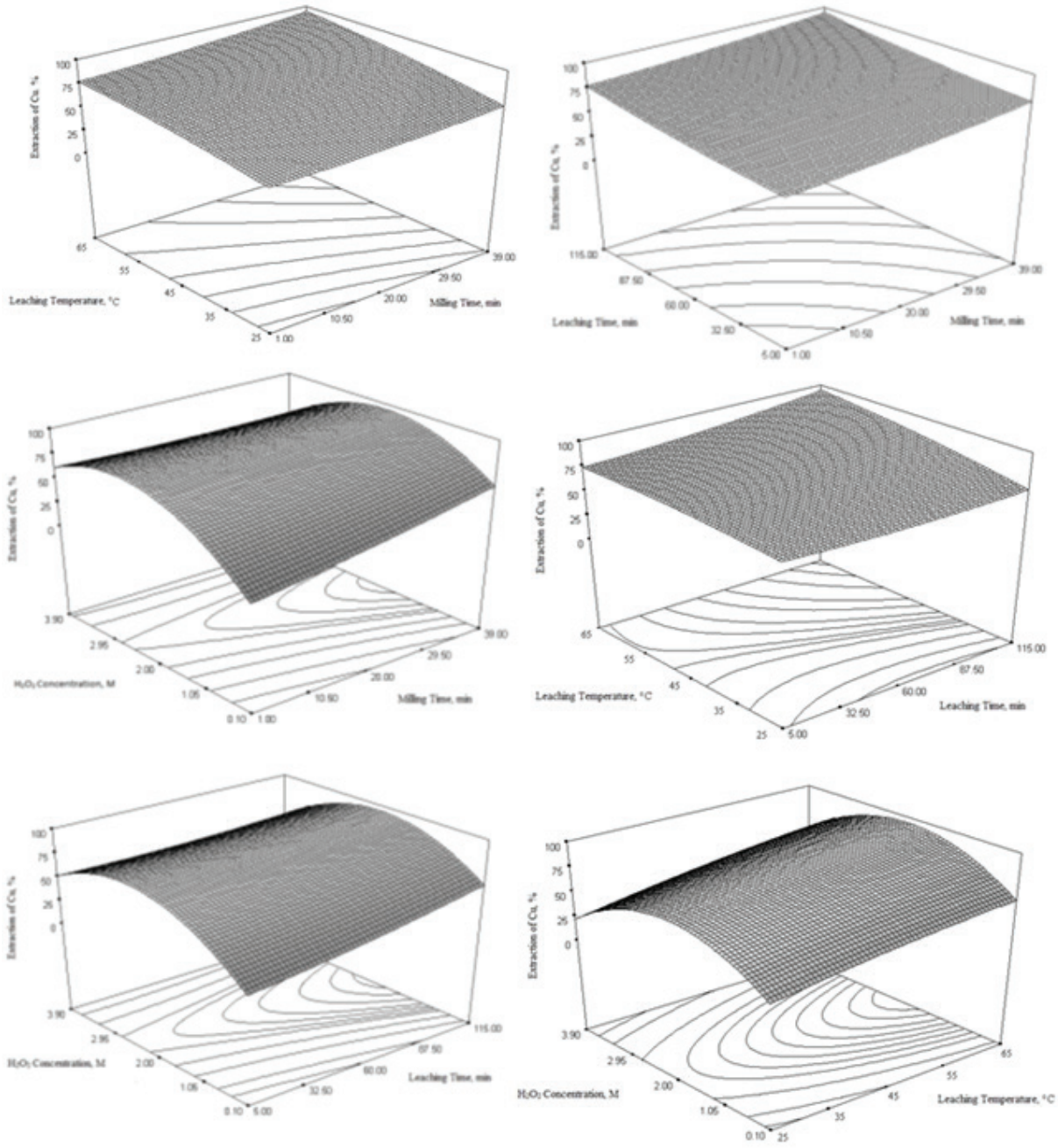

Figure 1. The interaction of various parameters on the copper extraction.

According to ANOVA results, it can be said that most effective parameter on the copper extraction is D^2 namely hydrogen peroxide concentration, so that when the peroxide concentration changes it is having exponential effect on the results.
The experimental results were evaluated and approximating functions of extraction percent of copper is obtained as shown in Eqs. (1).

$$\%Cu=-33.08+0.61288*A-0.1*B+0.45*C+60.62*D+4.83x10^{-3}*A^2+8.96x10^{-4}*B^2-7.01x10^{-3}*C^2-10.85*D^2-4.31x10^{-4}*A*B+5.28x10^{-3}*A*C-0.31*A*D+5.41x10^{-3}*B*C-0.07*C*D+0.06*C*D \quad (1)$$

References

Mahajan, V., Misra, M., Zhong, K., Fuerstenau, M C. 2007. Enhanced leaching of copper from chalcopyrite in hydrogen peroxide–glycol system. Hydrometallurgy, 20, 670-674.

McDonald, R G., Muir, D M. 2007a. Pressure oxidation leaching of chalcopyrite. Part I: Comparison of high and low temperature reaction kinetics and products. Hydrometallurgy, 86, 191–205.

McDonald, R G, Muir, D M. 2007b. Pressure oxidation leaching of chalcopyrite. Part II: Comparison of medium temperature kinetics and products and effect of chloride ion. Hydrometallurgy, 86, 206-220.

Padilla, R., Pavez, P., Ruiz, M C. 2008. Kinetics of copper dissolution from sulfidized chalcopyrite at high pressure in H2SO4-O2. Hydrometallurgy, 91, 113–120.

Padilla, R., Vega, D., Ruiz, M C. 2007. Pressure leaching of sulfidized chalcopyrite in sulfuric acid–oxygen media. Hydrometallurgy, 86, 80–88.

Makale Gönderim Tarihi:19.07.2016
Yayına Kabul Tarihi:02.09.2016

Effect of Mechanical Activation on Roasting of Celestite Ore

Raşit Sezer[1,2]*, İbrahim Göksel Hızlı[2,3], Ayşegül Bilen[2], Selim Ertürk [2], Cüneyt Arslan [2]
[1] *Karadeniz Technical University*
[2] *Istanbul Technical University*
[3] *Istanbul University*
**Corresponding Author: rasitsezer@gmail.com, rsezer@ktu.edu.tr*

Abstract
In this study, effect of mechanical activation in planetary ball mill and disc mill, on carbothermic reduction of celestite ore with coke was investigated. Celestite ore (96% $SrSO_4$) from Sivas district was blended with excess metallurgical coke and mechanically activated for 1, 5, 15 and 45 min. Mechanically activated blends were analyzed by Particle Size Analyzer, Thermal Gravimetric Analyzer (TGA), Differential Scanning Calorimetric Analyzer (DSC), and X-Ray Diffractometer (XRD). The finest particles were obtained at 45 min disc milling, of which d50 was 1.30 µm. TGA and DSC analyses showed that the reaction temperature was decreasing from 973°C to 892°C, by 1 min disc milling and 45 min planetary ball milling, respectively. XRD peaks broadened and peak intensities decreased by extending the mechanical activation time in both type of milling processes. All of the mechanically activated powders were roasted at 900, 1000, and 1100°C. According to XRD analyses; it is possible to see some peaks of strontium sulphide (SrS) after roasting at 900 and 1000°C, however, at 1100°C carbide formation is obtained.

Keywords: Celestite, Mechanical Activation, Roasting

1. Introduction

Strontium is commonly used for CRT TVs, hard ferrite magnets, phosphorescence materials, color pigments, special glasses and zinc electrolysis (Carrillo, Uribe et al. 1995, Castillejos, de la Cruz del et al. 1996). Until recently, strontium carbonate ($SrCO_3$) was used for CRT TVs 60-65% of 245,000 tones annual production capacity (Suárez-Orduña, Rendón-Angeles et al. 2007) but it falls flat nowadays (Owusu and Litz 2000).

Although feasible grade of celestite ore is 50-60% $SrSO_4$, celestite deposits in Turkey, Spain and Canada have more than 90% $SrSO_4$ (Martínez-L, Uribe S et al. 2003). Celestite deposits in Sivas, Akkaya district, operated by Barit Maden Türk A.Ş., has excellent quality $SrSO_4$ reserve. Celestite concentrate reaches 95-96% $SrSO_4$ after shaking table and jigging with impurities 3% $CaSO_4$, 0,5% $BaSO_4$, 0,5% SiO_2 and 0,5% Fe_2O_3 (Dogan, Koral et al. 2004).

$SrCO_3$ is usually produced from celestite although, there is only a few feasible natural $SrCO_3$ reserve. There are two different methods to produce $SrCO_3$ from celestite; direct decomposition method and black ash method. Direct decomposition method is sulfate ion change reaction in an carbonating aqueous media (Zhang and Saito 1997) as like sodium carbonate (Na_2CO_3) (Zoraga and Kahruman 2014), ammonium carbonate (NH_4CO_3) (Bingöl, Aydoğan et al. 2012) etc. Black ash method, the common method for producing $SrCO_3$, is two-step process; at first strontium sulphide (SrS) is produced by carbothermic reduction of celestite at 1000-1100°C (Halim, Ibrahim et al. 2009), then SrS is leached in water. Second step of the black ash method is the precipitation of $SrCO_3$ by Na_2CO_3 (Habashi, F.1997), CO_2 (Owusu and Litz 2000), or different carbonating agents (Erdemoğlu and Canbazoğlu 1998).

The present study aims to understand effect of mechanical activation of carbothermic reduction of celestite. For this purpose, black ash properties investigated by mechanically activated blends prepared from Turkish celestite ore.

2. Materials and Method

The starting material celestite ore was supplied from Barit Maden Türk A.Ş. (Sivas). Celestite ore –as received, is -2mm in size with a chemical composition of 95,5% $SrSO_4$, 3% $CaSO_4$, 0,5% $BaSO_4$, 0,5% SiO_2 and 0,5% Fe_2O_3. The metallurgical coke consists of 88% fixed carbon, 10% ash, 1% volatile compound and 1% sulphur. Two different types of mill were used for mechanical activation; Fritsch Pulversiette 6 planetary ball mill and a universal disc mill. Grinding media are made out of tungsten carbide (WC) and the ratio of grinding medium to solid material blend is 10/1. For planetary ball milling 10 mm diameter balls were used with 17 g celestite and 8 g metallurgical coke blends which have excess carbon. 250 g milling balls and 25 g blend were placed into a 250 ml WC bowl and rotation speed was set to 500 rpm. For disc milling, blends were prepared as the same stoichiometry but approximately 10 times heavier. Milling studies run with for 1, 5, 15, and 45 min as 5 min run and 2 min cooling intervals. Mechanically activated blends were analyzed by Malvern Mastersizer 2000 Particle Size Analyzer, X'pert Pro X-Ray Diffractometer and Linseis STA PT1600 TG-DSC/DTA Simultaneous Thermal Analyzer. 3 g specimens from all blends were tested by roasting in a lab scale muffle furnace at 900, 1000 and 1100°C for 2 hours in an air atmosphere.

3. Results and Discussion

Structural and thermal properties of the milled celestite and coke mixtures were investigated. Mechanically activated blends were roasted at three different temperatures and their structural properties were investigated.

3.1. Mechanical Activation

Effect of the milling time and the type on the particle size changes were investigated by Malvern Mastersizer (Fig.1). 45 min ball-milled blend is defined as the finest particles of which d50 is 1.30 µm and d_{10} is 0.11 µm. Considering the d_{50} values disc milling blends are grinded to 156.26 µm, 7.62 µm, 1.91 µm and 1.30 µm for 1min, 5 min, 15 min and 45 min, respectively and ball milled blends are 16.05 µm, 5.82 µm, 3.35 µm and 2.22 µm for 1 min, 5 min, 15 min and 45 min, respectively.

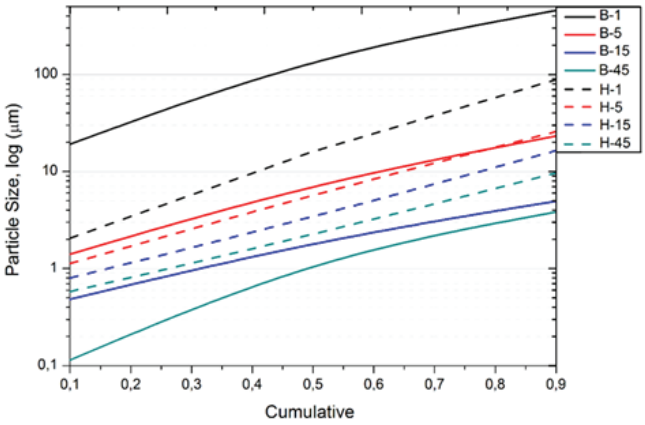

Figure 1. Particle size analyses of mechanically activated blends

X-Ray diffraction patterns of ball milled and disc milled blends and celestite ore as received are gathered for investigation of the structural changes by mechanical activation and shown in Fig.2. As a result of mechanical activation, peaks are broadening and intensities are decreasing by extending the milling time. Broadening and decreasing peak intensities are caused by disordering and thus obtaining partially amorphous structure. The highest peak of 1 min ball-milled blend is on 25.931° belongs to (002) but the other ball-milled (Fig.2.b) and the disc-milled (Fig.2.c) blends the highest peaks on 27.030° belongs to (210).

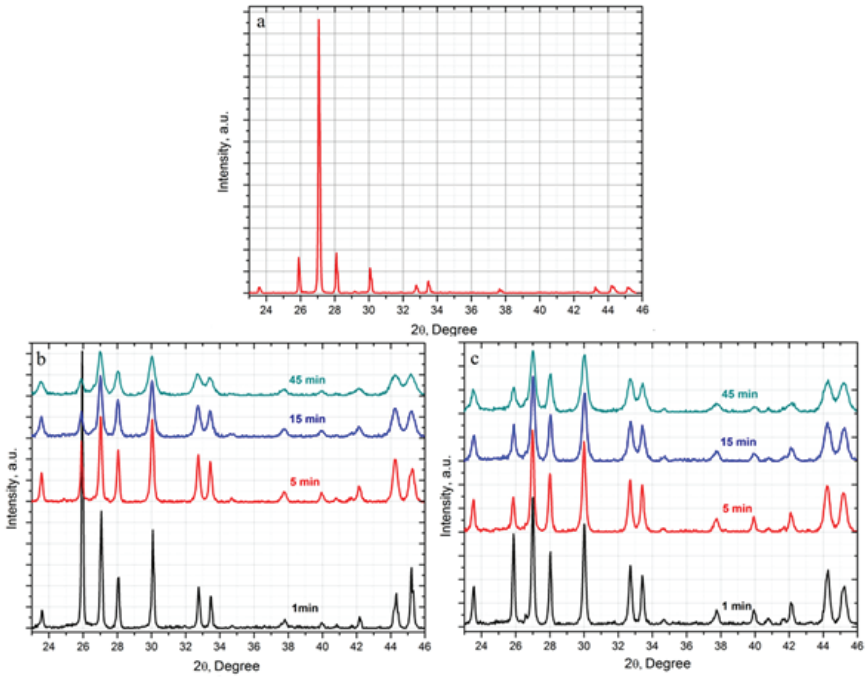

Figure 2. XRD patterns of received celestite (a) and mechanically activated celestite-coke blends; b) ball milled, c) disc milled

Thermal behaviors of mechanically activated celestite and coke mixtures were determined by DSC and TGA analyses, shown in Fig.3. The highest mass loses on the TG lines (Fig.3.b and Fig.3.d) and the pronounced sharp-cut on DSC lines of ball milled (Fig.3.a) and disc milled (Fig.3.c) blends, belong to the following carbothermic reduction reaction;

$$SrSO_4 + 2C \rightarrow SrS + 2CO_2 \quad (1)$$

According to this reaction strontium sulphur (SrS) occurs at the temperatures between 892°C and 973°C depends on the mechanical activation type and period. Reaction temperatures are decreasing from 965°C to 892°C by ball milling, and from 973°C to 915°C by disc milling.

The last and small peak at the DSC analyses means SrC2 occurrence temperature decrease by mechanical activation about the temperatures from 1100°C to 1050°C. Excessive amounts of carbon can cause the formation of SrC2 by the reaction with SrS at higher temperatures such as 1180°C (Erdemoğlu 2009). After reduction of celestite if there is some free carbon SrC2 occurs by the following reaction;

$$SrS + 2C \rightarrow SrC_2 + S° \quad (2)$$

Nevertheless, elemental sulphur was not detected in the roasted blends, by XRD analyses (Fig.4),

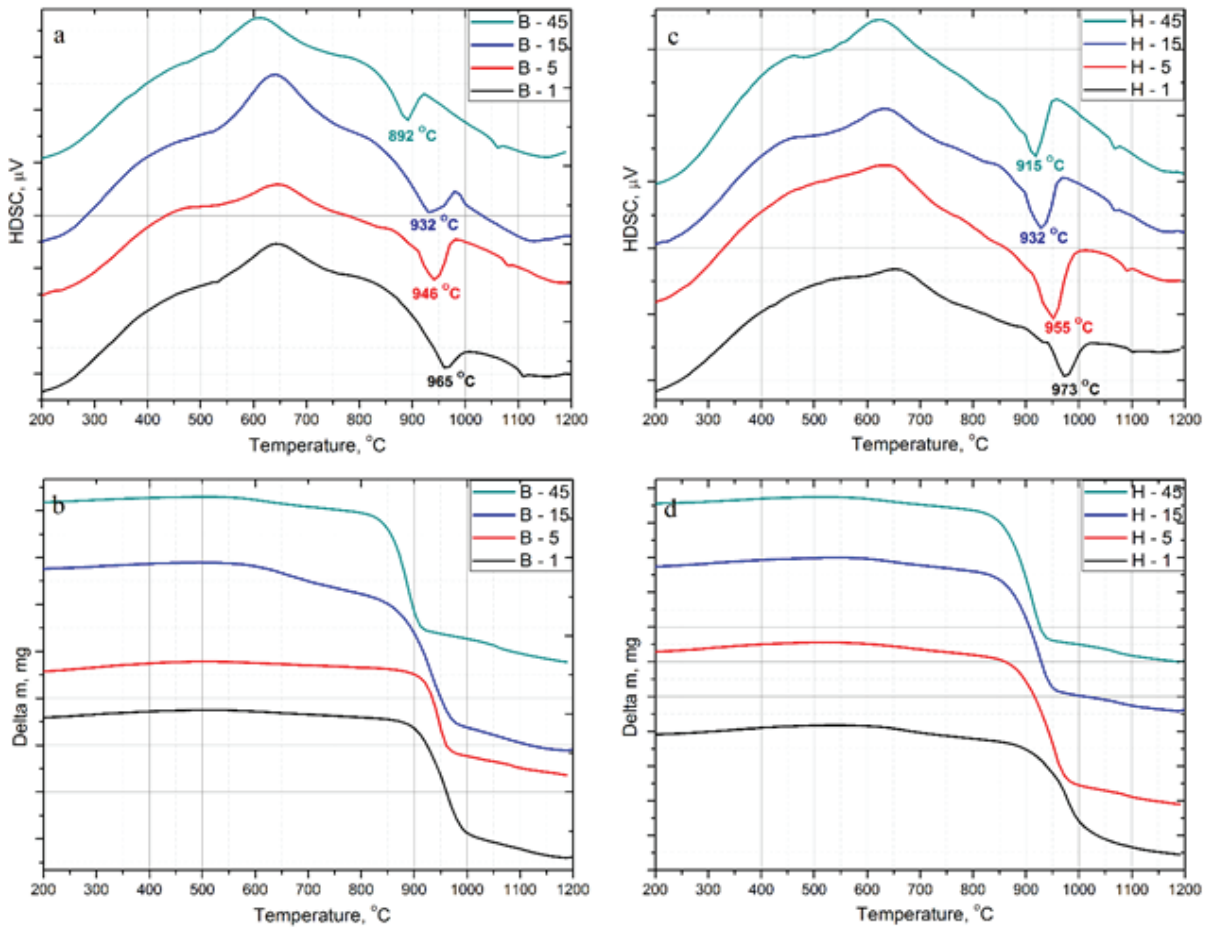

Figure 3. Thermal analyses of mechanically activated blends; a) DSC analyses of ball milled, b) TGA analyses of ball milled, c) DSC analyses of disc milled, d) TGA analyses of disc milled

3.2. Roasting

All mechanically activated blends were tested for roasting at different temperatures; 900, 1000, and 1100°C. -45µm celestite ore and coke mixture in the same proportion of the blends was roasted as non-activated
(0 min) blend to reference.

X-Ray analyses of activated and non-activated blends roasted at 900°C are given in Fig.4. However, there are no peaks belong to SrS for non-activated blends, peak intensities are increasing instantaneously by extending the mechanical activation period in both ball milling (Fig.4.a) and disc milling (Fig.4.b) processes. Whilst increasing the intensities of SrS peaks at 25.59°, 29.63° and 42.40°, intensities of the peaks belonging to the celestite are decreasing.

Under the light of X-Ray data SrS occur at 1000°C roasting regardless of mechanically activated and non-activated (Fig.4.c and 4.d.) On the other hand, depending on the activation time intensities of SrS peaks are increasing by extending mechanical activation time from 0 to 45 min.

According to XRD results of roasting test at 1100°C, the peaks defining SrS are decreasing by extending milling time and 15 min and 45 min ball milled (Fig.4.e) and 45 min disc milled (Fig.4.f) blends has no SrS peaks, despite non-activated blend has SrS peaks.

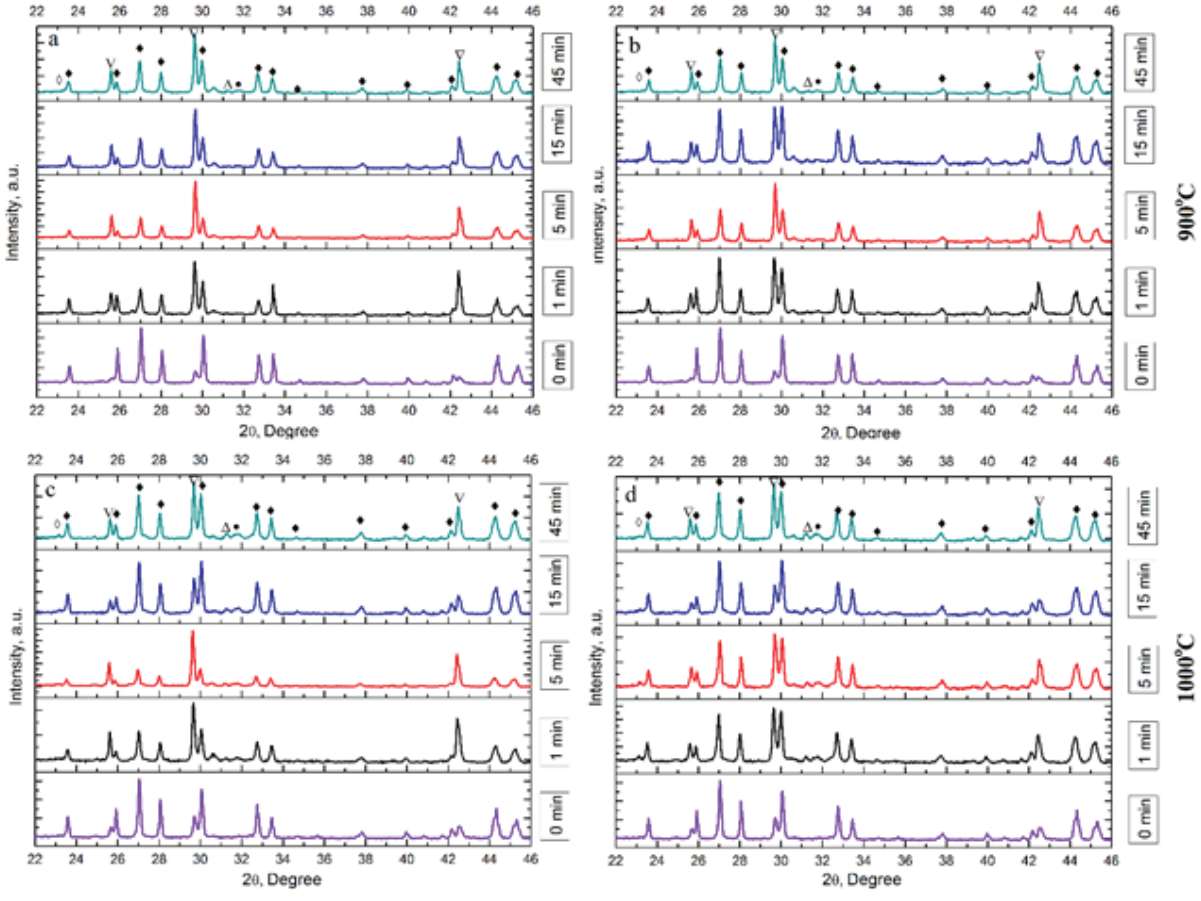

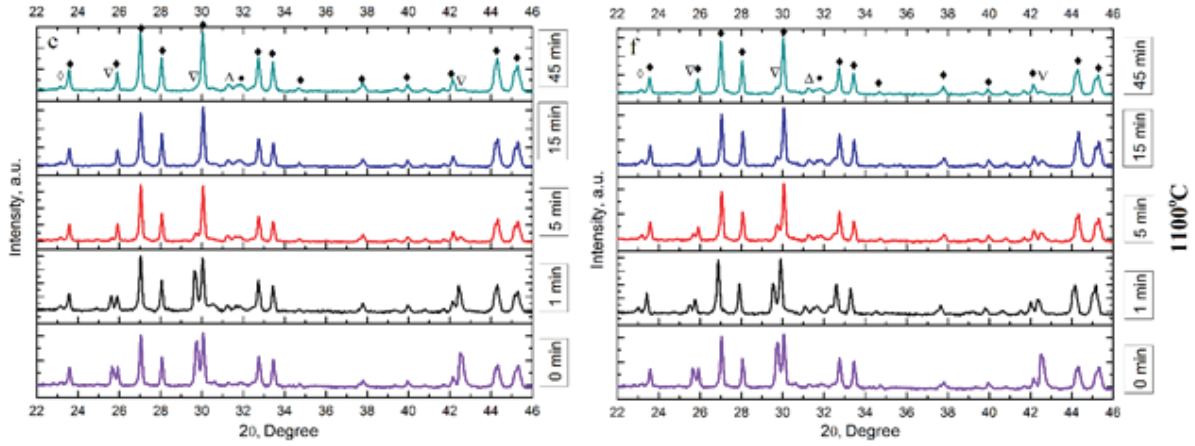

Figure 4. X-Ray analyses of roasted blends. ♦$SrSO_4$, ΔSrS, ●BaS, ◊BaC_2, ΔSrC_2

4. Conclusion

Black ash samples prepared from Turkish celestite and metallurgical coke mechanically activated by planetary ball milling and disc milling for short time up to 45 minutes. Particle size after milling processes is related to milling time and decreases by extending milling time. Mechanical activation causes distortions in $SrSO_4$ crystal structure so that XRD peaks are broadening and intensities decreasing by milling. During high energy milling of black ash blends no chemical reaction occurs to form SrS or any other compound. On the light of thermal analyses such as DSC and TGA, carbothermic reduction temperature decreases from 973°C to 892°C owing to the mechanical activation. The biggest exothermic peaks on DSC analyses and mass losses on TGA analyses point out the SrS occurrence temperature by the carbothermic reduction.

Roasting behavior of mechanically activated blends were tested at 900, 1000, and 1100°C. Mechanically activated blends have SrS at 900 and 1000°C, while non-activated blends have SrS at 1000 and 1100°C. Mechanical activation followed by roasting at 1100°C cause to occur SrC_2 and thus SrS cannot be seen.

As a result, mechanical activation can reduce the energy consumption of a high temperature processes; carbothermic reduction roasting of celestite. On the other hand, different activation systems can be experienced, because there is no remarkable difference between disc milled and ball milled activation.

Acknowledgement

The authors greatly acknowledge the financial support provided by Scientific and Research Council of Turkey (TUBITAK) under the contract no 115M631 and also we would like to thank to Barit Maden Türk A.Ş. for technical and materials support.

References

Bingöl, D., Aydoğan S., Bozbaş S. K., 2012. Production of $SrCO_3$ and (NH4)$2SO_4$ by the dry mechanochemical processing of celestite. Journal of Industrial and Engineering Chemistry, 18(2), 834-838.

Carrillo, F. R. P., Uribe A. S., Castillejos, A. H. E., 1995. A laboratory study of the leaching of celestite in a Pachuca tank. Minerals Engineering, 8(4–5), 495-509.

Castillejos, A. H. E., Cruz F. P. B., Uribe, A. S., 1996. The direct conversion of celestite to strontium carbonate in sodium carbonate aqueous media. Hydrometallurgy, 40(1–2), 207-222.

Dogan, H., Koral M., Kocakusak, S., 2004. Acid leaching of Turkish celestite concentrate. Hydrometallurgy, 71(3-4), 379-383.

Erdemoğlu, M., 2009. Carbothermic reduction of mechanically activated celestite. International Journal of Mineral Processing, 92(3–4), 144-152.

Erdemoğlu, M., Canbazoğlu, M., 1998. The leaching of SrS with water and the precipitation of $SrCO_3$ from leach solution by different carbonating agents. Hydrometallurgy, 49(1–2), 135-150.

Habashi, F., 1997, Handbook of Extractive Metallurgy, vol. 4, New York, Wiley – VCH, ISBN 3 – 527 – 28792 – 3, 2329 -2336.

Halim, K. S. A., Ibrahim S. S., El-Barawy, K. A., 2009. Isothermal reduction behaviour of celestite concentrate by solid carbon. Mineral Processing and Extractive Metallurgy, 118(4), 222-226.

Martínez-L, A., Uribe A.S., Carrillo F.R., Coreño A., Ortiz, J. C. , 2003. Study of celestite flotation efficiency using sodium dodecyl sulfonate collector: factorial experiment and statistical analysis of data. International Journal of Mineral Processing, 70(1–4), 83-97.

Owusu, G., Litz, J. E., 2000. Water leaching of SrS and precipitation of $SrCO_3$ using carbon dioxide as the precipitating agent. Hydrometallurgy, 57(1), 23-29.

Suárez-Orduña, R., Rendón-Angeles J. C., Yanagisawa, K., 2007. Kinetic study of the conversion of mineral celestite to strontianite under alkaline hydrothermal conditions. International Journal of Mineral Processing, 83(1–2), 12-18.

Zhang, Q., Saito, F., 1997. Mechanochemical processing of celestine. Chemical Engineering Journal, 66(1), 79-82.

Zoraga, M., Kahruman, C., 2014. Kinetics of conversion of celestite to strontium carbonate in solutions containing carbonate, bicarbonate and ammonium ions and dissolved ammonia. Journal of the Serbian Chemical Society, 79(3), 345-359.